3

Periodic solutions

3.1 Linear stability: Orr–Sommerfeld equation

Before applying the previously described numerical scheme we make some considerations about the equation of vorticity and linearized stability. It is known from vector calculus that the rotational of a vector field of velocities, i.e. the vorticity, is a vector field parallel to the rotation axis of the fluid, whose magnitude doubles that of the angular speed.

Vorticity equation. Firstly, we eliminate the pressure in the Navier–Stokes equations by applying the curl operator ($\boldsymbol{\nabla} \times \cdot$) to the momentum equation

$$\frac{\partial \mathbf{u}}{\partial t} + (\mathbf{u} \cdot \boldsymbol{\nabla})\mathbf{u} = -\nabla p + \frac{1}{Re}\boldsymbol{\Delta}\mathbf{u}, \tag{3.1}$$

where $\mathbf{u} = (u, v, 0)$ is the velocity field subjected to the incompressibility condition $\boldsymbol{\nabla} \cdot \mathbf{u} = 0$. Let us call $\boldsymbol{\omega} = \boldsymbol{\nabla} \times \mathbf{u}$, the vorticity vector. Given vectorial fields $F, G : \mathbb{R}^3 \longrightarrow \mathbb{R}^3$ the following formula holds

$$\operatorname{curl}(F \times G) = F \operatorname{div} G - G \operatorname{div} F + (G \cdot \boldsymbol{\nabla})F - (F \cdot \boldsymbol{\nabla})G,$$

where $\operatorname{div} F = \boldsymbol{\nabla} \cdot F$. This formula applied to $F = \mathbf{u}$ and $G = \boldsymbol{\omega}$ gives

$$\operatorname{curl}(\mathbf{u} \times \boldsymbol{\omega}) = \mathbf{u} \operatorname{div} \boldsymbol{\omega} - \boldsymbol{\omega} \operatorname{div} \mathbf{u} + (\boldsymbol{\omega} \cdot \boldsymbol{\nabla})\mathbf{u} - (\mathbf{u} \cdot \boldsymbol{\nabla})\boldsymbol{\omega} = (\boldsymbol{\omega} \cdot \boldsymbol{\nabla})\mathbf{u} - (\mathbf{u} \cdot \boldsymbol{\nabla})\boldsymbol{\omega},$$

now that $\mathbf{u}$ is a solenoidal field, $\operatorname{div} \mathbf{u} = 0$, and for all field $F : \mathbb{R}^3 \longrightarrow \mathbb{R}^3$, $\operatorname{div} \operatorname{curl} F = 0$. It is also straightforward to check that

$$\frac{1}{2}\nabla(\mathbf{u} \cdot \mathbf{u}) = \mathbf{u} \times \operatorname{curl} \mathbf{u} + (\mathbf{u} \cdot \boldsymbol{\nabla})\mathbf{u},$$

and because for every $f : \mathbb{R}^3 \longrightarrow \mathbb{R}$ we have $\operatorname{curl} \nabla f = 0$, then

$$\operatorname{curl}\left[(\mathbf{u} \cdot \boldsymbol{\nabla})\mathbf{u}\right] = -\operatorname{curl}(\mathbf{u} \times \operatorname{curl} \mathbf{u}) = (\mathbf{u} \cdot \boldsymbol{\nabla})\boldsymbol{\omega} - (\boldsymbol{\omega} \cdot \boldsymbol{\nabla})\mathbf{u}.$$

Finally it is easy to verify the identities

$$\operatorname{curl}\frac{\partial \mathbf{u}}{\partial t}=\frac{\partial}{\partial t}(\operatorname{curl}\mathbf{u})=\frac{\partial \boldsymbol{\omega}}{\partial t},\qquad \operatorname{curl}(\boldsymbol{\Delta}\mathbf{u})=\boldsymbol{\Delta}(\operatorname{curl}\mathbf{u})=\boldsymbol{\Delta}\boldsymbol{\omega},$$

and now we can apply curl to every term in (3.1) to get

$$\frac{\partial \boldsymbol{\omega}}{\partial t}+(\mathbf{u}\cdot\boldsymbol{\nabla})\boldsymbol{\omega}-(\boldsymbol{\omega}\cdot\boldsymbol{\nabla})\mathbf{u}=\frac{1}{Re}\Delta\boldsymbol{\omega}, \tag{3.2}$$

which constitutes the vorticity equation.

The stream function. If (u,v) are the components of a solenoidal field in two dimensions, i.e. $u_x+v_y=0$, then the ordinary differential equation

$$-v(x,y)\,\mathrm{d}x+u(x,y)\,\mathrm{d}y=0, \tag{3.3}$$

is clearly exact and therefore has a first integral $\psi=\psi(x,y)$, such that solutions of (3.3) can be expressed as $\psi(x,y)=c$ for some constant $c\in\mathbb{R}$, and furthermore $\psi_x=-v$, $\psi_y=u$. On the other hand, by the form of (3.3), we see that its solutions have tangent vector parallel to (u,v). Solutions of (3.3) can also be interpreted as trajectory lines generated by the vector field (u,v). These trajectories are called streamlines and ψ is the stream function, which is constant on streamlines as we have just mentioned.

Let us now describe how to get ψ from approximations of u and v. If we express u, v and ψ as truncated Fourier series

$$(u,v,\psi)(x,y,t)=\sum_{k=-N}^{N}(\hat{u}_k,\hat{v}_k,\hat{\psi}_k)(y,t)\mathrm{e}^{\mathrm{i}k\alpha x},$$

then conditions $\psi_x=-v$ and $\psi_y=u$ are translated to

$$\psi_x(x,y,t)=\sum_{k=-N}^{N}\mathrm{i}k\alpha\hat{\psi}_k(y,t)\mathrm{e}^{\mathrm{i}k\alpha x}=-\sum_{k=-N}^{N}\hat{v}_k(y,t)\mathrm{e}^{\mathrm{i}k\alpha x},$$
$$\psi_y(x,y,t)=\sum_{k=-N}^{N}\frac{\partial\hat{\psi}_k}{\partial y}(y,t)\mathrm{e}^{\mathrm{i}k\alpha x}=\sum_{k=-N}^{N}\hat{u}_k(y,t)\mathrm{e}^{\mathrm{i}k\alpha x},$$

and consequently

$$\hat{\psi}_k(y,t)=\begin{cases}\mathrm{i}\hat{v}_k(y,t)/(k\alpha), & k\neq 0,\\ \int\hat{u}_0(y,t)\,\mathrm{d}y, & k=0.\end{cases}$$

Now putting $\hat{u}_0$ and $\hat{\psi}_0$ as a truncated Chebyshev series

$$\hat{u}_0=\sum_{j=0}^{M}\tilde{u}_{0j}T_j(y),\qquad \hat{\psi}_0=\sum_{j=0}^{M}\tilde{\psi}_{0j}T_j(y),$$

we can reverse and adapt algorithm (2.9) to our case by

$$\tilde{\psi}_{0j+1} = \frac{c_j \tilde{u}_{0j} - \tilde{u}_{0j+2}}{2(j+1)}, \qquad j = 0, \dots, M.$$

For the vorticity in two dimensions it turns out that $\boldsymbol{\omega} = \boldsymbol{\nabla} \times (u, v, 0) = (0, 0, \omega)$, for $\omega = v_x - u_y$, and thus we can easily compute ω from u, v as

$$\omega(x, y, t) = \sum_{k=-N}^{N} \hat{\omega}_k(y, t) \mathrm{e}^{\mathrm{i}k\alpha x} = \sum_{k=-N}^{N} \left(\mathrm{i}k\alpha \hat{v}_k(y, t) - \frac{\partial \hat{u}_k}{\partial y}(y, t) \right) \mathrm{e}^{\mathrm{i}k\alpha x}.$$

In figures 3.1 and 3.2 we present surface level plots of stream function and vorticity, that is, curves $\psi = c$ and $\omega = c$ respectively for c constant. The highest vorticity level is attained close to the walls where there are more vortices, meanwhile the fluid is irrotational through a curve near the centre of the channel. Close to $y = 1$ the vorticity is mainly positive, which means that rotation is counter clock-wise, and the opposite happens close to $y = -1$.

Stability of the laminar solution. In two dimensions the vorticity vector $\boldsymbol{\omega} = (0, 0, \omega)$ satisfies $(\mathbf{u} \cdot \boldsymbol{\nabla})\boldsymbol{\omega} = 0$. The equation for ω is the third component of (3.2), namely

$$\omega_t + \psi_y \omega_x - \psi_x \omega_y = \frac{1}{Re} \Delta \omega, \tag{3.4}$$

where $\psi = \psi(x, y, t)$ is the previously defined stream function. Equation (3.4) is also known as the Helmholtz form of the Navier–Stokes equations. The stream function ψ_b associated to the laminar flow $(u_b, v_b) = (1 - y^2, 0)$, is $\psi_b(y) = y - y^3/3$, obtained by integration of u_b. To study the stability of ψ_b, we perturb it by considering $\psi = \psi_b + \varepsilon \hat{\psi}$, for ε a small parameter and $\hat{\psi} = \hat{\psi}(x, y, t)$ a perturbation of ψ_b. Substituting $\omega = -\Delta\psi$ in (3.4) it results

$$\Delta\psi_t + \psi_y \Delta\psi_x - \psi_x \Delta\psi_y = \frac{1}{Re} \Delta^2 \psi,$$

which can be put in terms of $\hat{\psi}$ as

$$\Delta\hat{\psi}_t + (u_b + \varepsilon\hat{\psi}_y)\Delta\hat{\psi}_x - \hat{\psi}_x(u_b'' + \varepsilon\Delta\hat{\psi}_y) = \frac{1}{Re} \Delta^2 \hat{\psi}.$$

At this point we neglect quadratic terms in $\hat{\psi}$ to obtain a linear problem

$$\Delta\hat{\psi}_t + u_b \Delta\hat{\psi}_x - u_b'' \hat{\psi}_x = \frac{1}{Re} \Delta^2 \hat{\psi}. \tag{3.5}$$

We simplify the perturbing function $\hat{\psi}$ by separating temporal and spatial variables as $\hat{\psi} = \exp(\lambda t)\xi(x, y)$, for $\lambda \in \mathbb{C}$, which substituted in (3.5) gives rise to the spectral problem

$$\lambda\Delta\xi + u_b \Delta\xi_x - u_b'' \xi_x = \frac{1}{Re} \Delta^2 \xi. \tag{3.6}$$

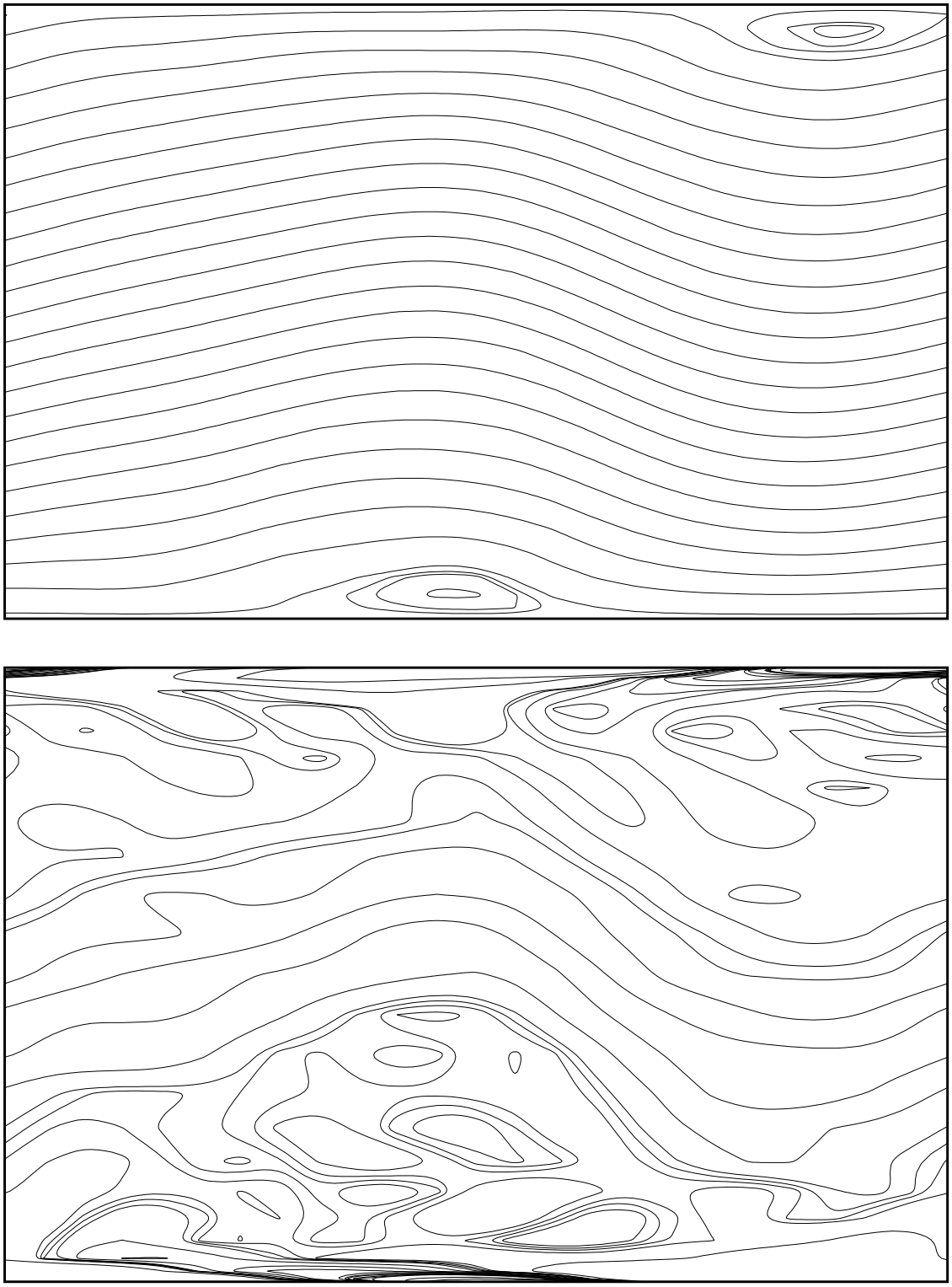

FIGURE 3.1. Surface levels of stream function and vorticity respectively in $[0, L] \times [-1, 1]$ for flow a in table 2.3.

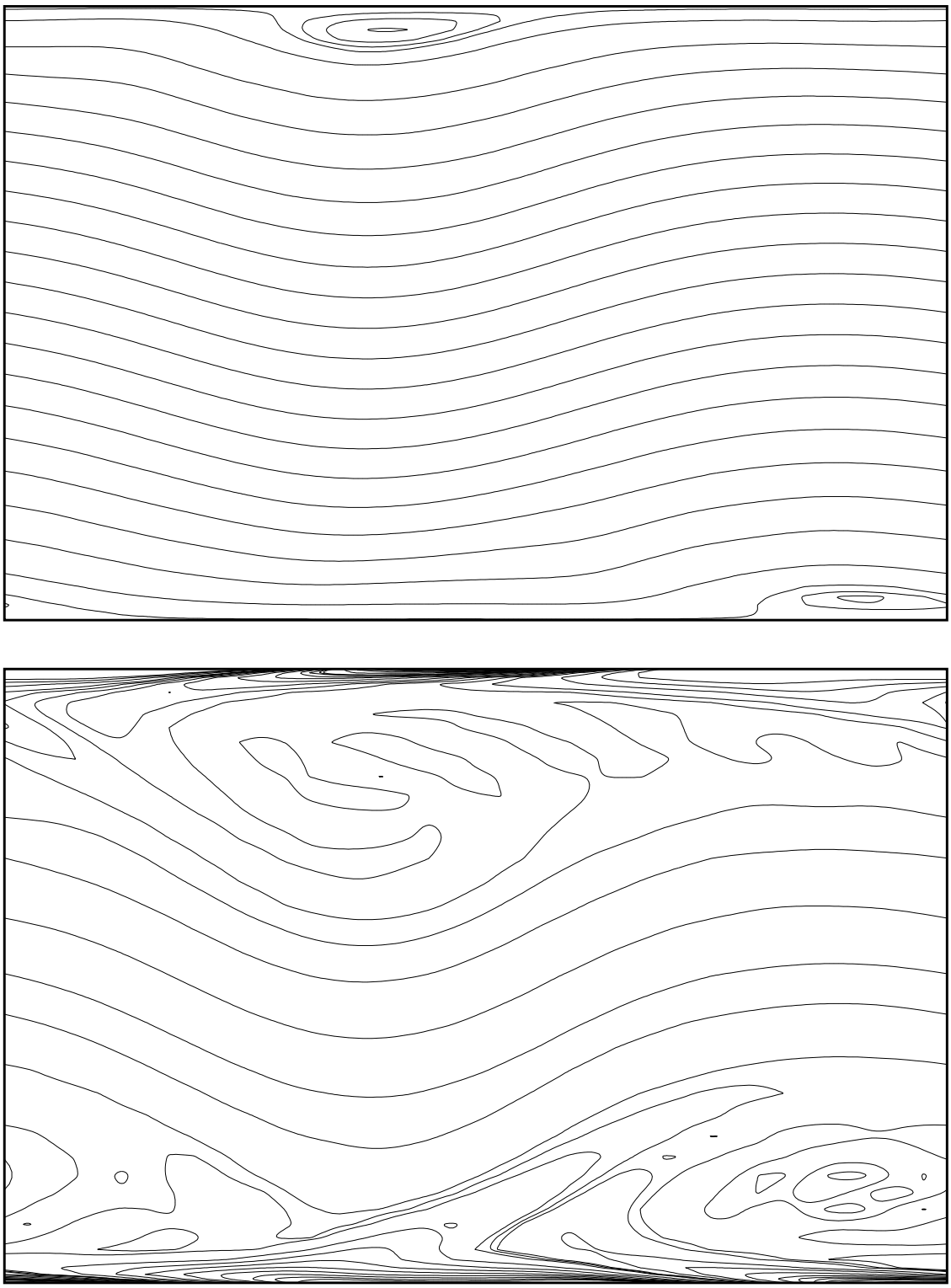

FIGURE 3.2. Analogous to fi gure 3.1 for fbw c in table 2.3.

Now the stability of ψ_b means that for every perturbation $\hat{\psi} = \exp(\lambda t)\xi(x,y)$ for $\xi \neq 0$, which satisfies (3.6), it must be $\mathrm{Re}(\lambda) < 0$. Otherwise ψ_b is a neutral stable for $\mathrm{Re}(\lambda) = 0$, or an unstable solution if $\mathrm{Re}(\lambda) > 0$.

Due to boundary conditions (1.6) we consider $\hat{\psi}$ a $2\pi/\alpha$-periodic function in x for $\alpha = 2\pi/L$, which is equivalent to ξ be a $2\pi/\alpha$-periodic function and thus we may express it as a Fourier series

$$\xi(x,y) = \sum_{k\in\mathbb{Z}} \hat{\xi}_k(y)\mathrm{e}^{\mathrm{i}k\alpha x}.$$

Since (3.6) is a linear problem we may suppose that it is satisfied by each of the terms $\hat{\xi}_k(y)\mathrm{e}^{\mathrm{i}k\alpha x}$, or generalizing, by any function of type $\xi(x,y) = \phi(y)\mathrm{e}^{\mathrm{i}\alpha x}$, which substituted in (3.6) yields

$$(\mathrm{i}\alpha u_b + \lambda)(\phi'' - \alpha^2\phi) - \mathrm{i}\alpha u_b''\phi = \frac{1}{Re}(\phi^{(4)} - 2\alpha^2\phi'' + \alpha^4\phi), \tag{3.7}$$

a fourth order ordinary differential equation on ϕ, known as the Orr–Sommerfeld equation. Since we suppose $\psi(x,y,t) = \psi_b(y) + \varepsilon\exp(\lambda t)\phi(y)\exp(\mathrm{i}\alpha x)$, it turns out

$$u = \psi_y = u_b(y) + \varepsilon\phi'(y)\mathrm{e}^{\mathrm{i}\alpha x+\lambda t}, \qquad v = -\psi_x = \varepsilon\mathrm{i}\alpha\phi(y)\mathrm{e}^{\mathrm{i}\alpha x+\lambda t},$$

and then from (1.6)

$$u(x,\pm1,t) = v(x,\pm1,t) = 0 \quad\Longleftrightarrow\quad \phi'(\pm1) = \phi(\pm1) = 0, \tag{3.8}$$

we obtain boundary conditions for ϕ, which together with (3.7) represent an eigenvalue problem for Re, α, λ and the eigenfunction ϕ. Fixing values of Re and α, we search for $\lambda = \lambda_r + \mathrm{i}\lambda_i$ such that there exist an eigenfunction $\phi \neq 0$ which satisfies (3.7)–(3.8). If for such λ it results $\lambda_r > 0$, then the laminar flow is unstable to small disturbances according to the linear theory. If it always happens to be $\lambda_r < 0$ then the laminar flow is stable. If there exists λ such that $\lambda_r = 0$, and for the remaining eigenvalues $\lambda_r < 0$, then the laminar flow is said to be neutrally stable.

Numerical solution of the Orr–Sommerfeld equation. We have employed finite differences to approximate $\phi(y)$ and its derivatives in order to approximate the solution of (3.7)–(3.8). We take a uniform mesh $y_k = kh - 1 \in [-1,1]$ for $h = 2/(Q+1)$, Q positive integer sufficiently large and $k = 0,\ldots,Q+1$. After putting $\phi_k = \phi(y_k)$ we estimate derivatives as

$$\phi''(y_k) \approx \phi_k'' = \frac{\phi_{k+1} - 2\phi_k + \phi_{k-1}}{h^2}, \qquad \text{for } k = 1,\ldots,Q$$

$$\phi^{(4)}(y_k) \approx \phi_k^{(4)} = \frac{1}{h^4}\begin{cases} 2(2\phi_3 - 9\phi_2 + 18\phi_1)/3, & \text{for } k = 1 \\ \phi_{k+2} - 4\phi_{k+1} + 6\phi_k - 4\phi_{k-1} + \phi_{k-2}, & \text{for } k = 2,\ldots,Q-1 \\ 2(18\phi_Q - 9\phi_{Q-1} + 2\phi_{Q-2})/3, & \text{for } k = Q. \end{cases}$$

The formula of ϕ_k'' for $k = 1,\ldots,Q$ is obtained from the second derivative of the interpolating polynomial of ϕ at y_{k-1}, y_k and y_{k+1}. For the particular cases $k = 1, Q$, we utilize the same formula, bearing in mind that from (3.8) it is $\phi_0 = \phi_{Q+1} = 0$. The same idea applies to $\phi_k^{(4)}$ for $k = 2,\ldots,Q-1$ using the fourth derivative of the interpolating polynomial of ϕ at y_{k-2}, y_{k-1}, y_k, y_{k+1} and y_{k+2}. To approximate $\phi^{(4)}(y_1)$, we derivate four times the Hermite interpolating

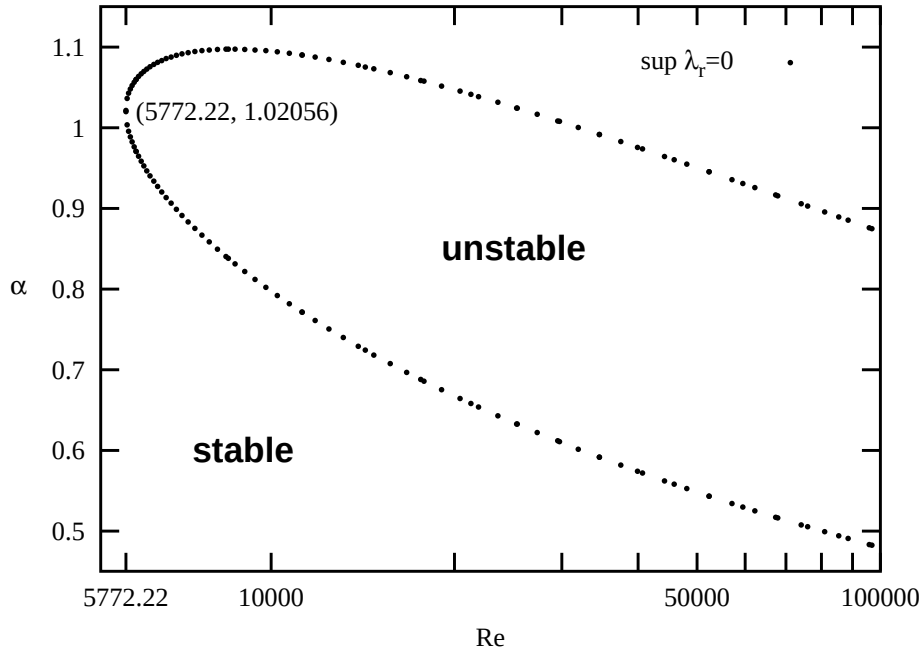

FIGURE 3.3. Neutral stability curve for the laminar solution. For each point in this curve the most unstable eigenvalue λ is purely imaginary. The critical Reynolds number is attained at $Re_{cr} = 5772.22$. The curve splits the Re-α plain in two stability regions as shown in the graph. For $\alpha \geqslant 1.1$ the laminar flow is linearly stable for every Re.

polynomial of $\phi(y_0)$, $\phi(y_1)$, $\phi(y_2)$, $\phi(y_3)$ and $\phi'(y_0)$. Analogously for $\phi^{(4)}(y_Q)$ at $\phi(y_{Q-2})$, $\phi(y_{Q-1})$, $\phi(y_Q)$, $\phi(y_{Q+1})$ and $\phi'(y_{Q+1})$. Due to (3.8) we impose $\phi'(y_0) = \phi'(y_{Q+1}) = 0$.

The substitution of ϕ_k, ϕ_k'' and $\phi_k^{(4)}$ in (3.7) for $k = 1, \ldots, Q$ yields

$$\frac{1}{Re}(\phi_k^{(4)} - 2\alpha^2\phi_k'' + \alpha^4\phi_k) - \mathrm{i}\alpha u_b(y_k)(\phi_k'' - \alpha^2\phi_k) - 2\mathrm{i}\alpha\phi_k = \lambda(\phi_k'' - \alpha^2\phi_k),$$

an eigenvalue problem of dimension Q of form $A\phi = \lambda B\phi$, where A, B are matrices which only depend on Re, α, and Q. Matrix A is pentadiagonal and B tridiagonal. We are only interested on the most unstable eigenvalue, i.e. λ with the highest real part. We calculate it by means of the power method. To this end we put $\phi^0 = (1, \ldots, 1)^t$, and for $n = 0, 1, 2, \ldots$, we follow the recurrence

$$(A - qB)\bar{\phi}^{n+1} = B\phi^n, \qquad \phi \approx \phi^{n+1} = \frac{\bar{\phi}^{n+1}}{\|\bar{\phi}^{n+1}\|_\infty}, \qquad \mu_{n+1} = \frac{\bar{\phi}_m^{n+1}}{\phi_m^n}, \qquad \lambda \approx \frac{1}{\mu_{n+1}} + q,$$

where m is selected such that $\|\bar{\phi}^{n+1}\|_\infty = |\bar{\phi}_m^{n+1}|$. The recurrence consist of the application of the power method to the matrix $(A - qB)^{-1}B = (B^{-1}A - qI)^{-1}$, which furnishes the eigenvalue of $B^{-1}A$ closest to q. We vary q in order to accelerate the convergence of the power method. Likewise, given mesh sizes h and $h/2$, we calculate $\lambda(h)$ and $\lambda(h/2)$, and by means of an algorithm analogous to (2.31) we extrapolate the value of λ to improve its precision.

The results obtained by this algorithm are reported by other authors, e.g. the classical work of Orszag (1971). The neutral stability curve, $\lambda_r = 0$, is presented in figure 3.3. In this figure,

each point in the Re-α plane represents a perturbation of the laminar solution whose stability is decided upon its position. We also observe the critical Reynolds number, $Re_{cr} = 5772.22$ for $\alpha = 1.02056$, so that if $Re < Re_{cr}$ the laminar solution is linearly stable for any value of α. As an advantage of the preceding algorithm compared to the spectral approach designed in Orszag (1971), can be emphasized its easiness of implementation. Taking $Q < 1000$ we have achieved a precision analogous to the one in Orszag (1971).

3.2 Reduction of periodic orbits to stationary solutions

With the help of the results in appendix A, the obtaining of time periodic solutions is reduced to the search of fixed points. These are computed from an algebraic system of equations, for different values of parameters Re and α. This variation of parameters is carried out by pseudo-arclength continuation, a method whose main guidelines are described in §2.8.

By observing figure 3.3 we may select a point (Re, α) for which the laminar solution is unstable according to (3.7). For instance, if we take $\alpha = 1.02056$ and $Re = 6000$, the laminar flow is unstable and hence a small perturbation, after some time of evolution, will lead the fluid to a different attracting state. Unless mentioned explicitly the time evolution of the fluid is observed in a steady frame of reference, i.e. $c = 0$ in (1.7). In order to accelerate the approach to the new attracting flow, the perturbation of the laminar flow is based on the most unstable eigensolution of the Orr–Sommerfeld equation (3.7). Precisely, taking $\phi(y)$ as the solution of (3.7) associated to λ with $\mathrm{Re}(\lambda) > 0$, the effective perturbation is given by

$$u = u_b(y) + \varepsilon \mathrm{Re}\left(\phi'(y)\mathrm{e}^{\mathrm{i}\alpha x + \lambda t}\right), \qquad v = \varepsilon \mathrm{Re}\left(\mathrm{i}\alpha\phi(y)\mathrm{e}^{\mathrm{i}\alpha x + \lambda t}\right).$$

The Poincaré section Σ_1 defined in §2.7 allows us to study this new attracting state of the fluid. Comparing two consecutive crossings of the fluid through Σ_1, we observe that the discretized coefficients of the velocity $U = (u_0, \bar{u}_1, \ldots, \bar{u}_N)$ coincides within a reasonable precision depending on Δt. We conclude that the new attracting state is a time-periodic orbit, whose period T is easily calculated from the time elapsed between two consecutive crossings of Σ_1.

As in the remarks following definition A.4 we set $R_\theta(u(x, y, t)) = u(x - \theta, y, t)$, as a translation of $\theta \in \mathbb{R}$ in the stream direction x. Although in the following considerations we only mention u, the same ideas apply for v and p. In addition, boundary conditions (1.6) are always supposed. We now may apply theorem A.12 to our new periodic flow $u(x, y, t)$ of period T, to deduce that $u(x, y, t)$ is a rotating (or travelling) wave as in definition A.10, i.e.

$$u(x, y, t) = u(x - ct, y, 0), \quad c = L/T. \tag{3.9}$$

In this case $m = 1$ is the order of axisymmetry of the wave. The value of c is obtained from lemma A.11. If we set $\tilde{x} = x - ct$ as the coordinate in the stream direction for an observer who is moving at speed c and $\tilde{u}(\tilde{x}, y, t) = u(\tilde{x} + ct, y, t)$ as the corresponding velocity in the moving frame, then using property (3.9) we have

$$\tilde{u}(\tilde{x}, y, t) = u(\tilde{x} + ct, y, t) = u(\tilde{x}, y, 0) = \tilde{u}(\tilde{x}, y, 0). \tag{3.10}$$

This means that in a system of reference moving at speed c, $u(x,y,t)$ is observed as a stationary solution, and consequently $\tilde{u}(\tilde{x},y)$ solves the stationary version of (1.7),

$$\begin{cases} (\tilde{u}-c)\dfrac{\partial\tilde{u}}{\partial\tilde{x}}+\tilde{v}\dfrac{\partial\tilde{u}}{\partial y}=-\dfrac{\partial\tilde{p}}{\partial\tilde{x}}+\dfrac{1}{Re}\left(\dfrac{\partial^2\tilde{u}}{\partial\tilde{x}^2}+\dfrac{\partial^2\tilde{u}}{\partial y^2}\right) \\ (\tilde{u}-c)\dfrac{\partial\tilde{v}}{\partial\tilde{x}}+\tilde{v}\dfrac{\partial\tilde{v}}{\partial y}=-\dfrac{\partial\tilde{p}}{\partial y}+\dfrac{1}{Re}\left(\dfrac{\partial^2\tilde{v}}{\partial\tilde{x}^2}+\dfrac{\partial^2\tilde{v}}{\partial y^2}\right) \\ \dfrac{\partial\tilde{u}}{\partial\tilde{x}}+\dfrac{\partial\tilde{v}}{\partial y}=0. \end{cases} \tag{3.11}$$

Conversely if $\tilde{u}(\tilde{x},y)$ is a solution of (3.11), by defining $u(x,y,t)=\tilde{u}(x-ct,y)$, it results a T-periodic flow on time for $T=L/c$, solution of (1.5). Indeed, bearing in mind the L-periodicity of $\tilde{u}$ in $\tilde{x}$, we have

$$u(x,y,t+T)=\tilde{u}(x-ct-cT,y)=\tilde{u}(x-ct-L,y)=\tilde{u}(x-ct,y)=u(x,y,t).$$

In this way travelling waves gives rise to stationary solutions of (3.11) and reciprocally. Since $u(x,y,t)$ is mL-periodic in x and nT-periodic in t for every $m,n\in\mathbb{Z}$, provided $u(x,y,t)$ is L-periodic in x and T-periodic in t, then, $c=mL/(nT)$ satisfies also (3.9) for every $m,n\in\mathbb{Z}$.

Fourier coefficients. Let us now look at a travelling wave in terms of discretized coefficients. If we put a travelling wave $u(x,y,t)$ and its transformed version $\tilde{u}(x,y,t)$, expanded in Fourier series

$$u(x,y,t)=\sum_{k\in\mathbb{Z}}\hat{u}_k(y,t)\mathrm{e}^{\mathrm{i}k\alpha x},\qquad \tilde{u}(\tilde{x},y,t)=\sum_{k\in\mathbb{Z}}\hat{\tilde{u}}_k(y,t)\mathrm{e}^{\mathrm{i}k\alpha\tilde{x}},$$

we find

$$\tilde{u}(\tilde{x},y,t)=u(\tilde{x}+ct,y,t)=\sum_{k\in\mathbb{Z}}\mathrm{e}^{\mathrm{i}k\alpha ct}\hat{u}_k(y,t)\mathrm{e}^{\mathrm{i}k\alpha\tilde{x}}.$$

Equating harmonics in the two series of $\tilde{u}(\tilde{x},y,t)$ and from (3.10) also with the harmonics of $\tilde{u}(\tilde{x},y,0)$, for every $k\in\mathbb{Z}$ we obtain

$$\hat{u}_k(y,t)=\mathrm{e}^{-\mathrm{i}k\alpha ct}\hat{\tilde{u}}_k(y,t)=\mathrm{e}^{-\mathrm{i}k\alpha ct}\hat{\tilde{u}}_k(y,0).$$

In particular for $k=0$ it turns out $\hat{u}_0(y,t)=\hat{\tilde{u}}_0(y,0)$ for all t. This means that, for a rotating wave $u(x,y,t)$, $\hat{u}_0(y,t)=\hat{u}_0(y)$, i.e. it does not depend on time. In this case, according to formulae (1.8) and (1.9), the flux through the channel Q and the average pressure gradient G are given by

$$Q=\int_{-1}^{1}\hat{u}_0(y)\,\mathrm{d}y,\qquad G=-\frac{1}{2Re}\left[\frac{\partial\hat{u}_0}{\partial y}\right]_{-1}^{1},$$

and so they remain constant on time for this kind of flow. A rotating wave is thus a secondary flow as defined in §1.6.

Periodic solutions for different flow conditions. Let us suppose that $\tilde{u}(\tilde{x}, y) = u^p(\tilde{x}, y)$ is a solution of (3.11) for $Re = Re_p$ defined in terms of a constant mean pressure gradient G. Because $u^p(\tilde{x}, y)$ is a secondary flow, as we have seen in (1.12), $u^Q(\tilde{x}, y) = ru^p(\tilde{x}, y)$ for $r = Re_p/Re_Q$ is the corresponding secondary flow when the scaling is defined by means of Re_Q and likewise $p^p(\tilde{x}, y) = r^2 p^Q(\tilde{x}, y)$ is the relation between pressures according to (1.13). The expression for r was established in (1.10) and (1.11). From those relations we easily obtain the respective ones among derivatives, which carried to (3.11) and simplified, translate to

$$\begin{cases} (u^Q - rc)\dfrac{\partial u^Q}{\partial \tilde{x}} + v^Q \dfrac{\partial u^Q}{\partial y} = -\dfrac{\partial p^Q}{\partial \tilde{x}} + \dfrac{1}{Re_Q}\left(\dfrac{\partial^2 u^Q}{\partial \tilde{x}^2} + \dfrac{\partial^2 u^Q}{\partial y^2}\right) \\ (u^Q - rc)\dfrac{\partial v^Q}{\partial \tilde{x}} + v^Q \dfrac{\partial v^Q}{\partial y} = -\dfrac{\partial p^Q}{\partial y} + \dfrac{1}{Re_Q}\left(\dfrac{\partial^2 v^Q}{\partial \tilde{x}^2} + \dfrac{\partial^2 v^Q}{\partial y^2}\right) \\ \dfrac{\partial u^Q}{\partial \tilde{x}} + \dfrac{\partial v^Q}{\partial y} = 0. \end{cases}$$

Hence since $u^Q(\tilde{x}, y)$ is a stationary solution of a system analogous to (3.11) then $u(x, y, t) = u^Q(x - rct, y)$ is a rotating wave with rc as the speed of the observer in the x direction. Therefore we only need to find periodic solutions as a stationary points for the case of constant mean pressure gradient, because by the previous arguments we can convert those solutions to periodic solutions of constant flux. The process, of course, can be reversed.

3.3 Continuation of periodic solutions

We are going to describe how to find numerically time periodic solutions which, as we have seen in §3.2, can be searched for as solutions of (3.11). The spatial discretization of (3.11), according to (2.22), is expressed as

$$0 = \mathcal{L}_k(\bar{u}_k) + \mathcal{N}_k(\bar{u}_0, \ldots, \bar{u}_N), \quad k = 0, \ldots, N, \tag{3.12}$$

where the modifications of §2.5 must be introduced for the constant flux case. The dimension of system (3.12) is $K = (2N + 1)(M - 2)$ or $K = (2N + 1)(M - 2) + 1$ for the constant flux or constant mean pressure gradient respectively. In addition (3.12) depends on parameters Re, α and c. In the following we consider the value of α fixed. As is easily verified, if $\tilde{u}(\tilde{x}, y)$ (together with $\tilde{v}$ and $\tilde{p}$) is a stationary solution of (3.11) then $\tilde{u}(\tilde{x} - \theta, y)$ also solves (3.11) for all $\theta \in \mathbb{R}$. Analogously, if $u(x, y, 0)$ is the starting position of a rotating wave with c as the corresponding velocity of the observer then, by (3.9), for every $\theta \in \mathbb{R}$ we have $u(x - \theta, y, 0) = u(x, y, \theta/c)$, and thus $u(x - \theta, y, 0)$ lies in the same orbit as $u(x, y, 0)$ and both satisfies (3.12). This property introduces a non-uniqueness in the solutions of (3.12) for fixed values of Re and c. In order to avoid it we fix a coordinate in $U = (\bar{u}_0, \ldots, \bar{u}_N)$, which is equivalent to select θ in the translated solution $\tilde{u}(\tilde{x} - \theta, y)$. We have considered the same coordinate fixed to 0 in all solutions of (3.12) to achieve continuity in the continuation process. This is equivalent to the restriction of the periodic solution to be in Σ_1, as defined in §2.7 for $s_1 = 0$. System (3.12) can expressed by a function

$$H : \gamma \in \mathbb{R}^{K+1} \longrightarrow H(\gamma) \in \mathbb{R}^K,$$

where K is as given above according to constant flux or pressure and $\gamma = (Re, c, \bar{u}_0, \ldots, \bar{u}_N)$ excluding the coordinate fixed to 0 in U. Thus we consider solutions of (3.11) as points in the curve $H^{-1}(0)$. We are in a position to apply the ideas of §2.8.

In §3.2 we explain how to obtain a time-periodic solution by perturbing the unstable laminar flow for a proper Re. We utilize this solution as a first approximated point of $H^{-1}(0)$. We improve its accuracy by means of corrector iterations (2.39) until we are close enough to $H^{-1}(0)$. At this point we can traverse the curve of periodic flows by means of continuation. To represent this family of periodic solutions we define its amplitude A, as the distance of the periodic solution (u, v) to the laminar profile $(u_b, 0)$, i.e.

$$A = \|(u - u_b, v)\|, \tag{3.13}$$

where the norm was defined in (2.34).

Lemma 3.1. *For a T-periodic flow $u(x, y, t)$, its amplitude does not depend on time.*

Proof: For a fixed $t \in \mathbb{R}$ one has

$$\int_0^L \int_{-1}^1 u(x,y,t)^2 \,\mathrm{d}y \,\mathrm{d}x \overset{1}{=} \int_0^L \int_{-1}^1 u(x-ct,y,0)^2 \,\mathrm{d}y \,\mathrm{d}x$$
$$\overset{2}{=} \int_{-ct}^{L-ct} \int_{-1}^1 u(\tilde{x},y,0)^2 \,\mathrm{d}y \,\mathrm{d}\tilde{x} \overset{3}{=} \int_0^L \int_{-1}^1 u(\tilde{x},y,0)^2 \,\mathrm{d}y \,\mathrm{d}\tilde{x}.$$

Step 1: By (3.9).
Step 2: Making the change of variable $\tilde{x} = x - ct$.
Step 3: Because u is L-periodic in x.
From definition (3.13) the result follows. □

For each solution of $H^{-1}(0)$ we plot in figures 3.4 and 3.5 its constant amplitude A as a function of Re_p or Re_Q respectively for $\alpha = 1.1$. Given a periodic solution based on Re_p, using formulas (1.10) or (1.11), together with (1.12) we obtain the corresponding periodic flow when the scaling is made in terms of Re_Q. We also observe in both figures 3.4 and 3.5 that the curve of periodic flows for $\alpha = 1.1$ never reaches the laminar flow for any Re. Starting at $Re \approx 9000$, the amplitude on the lower branch grows on increasing Re. This is in agreement with the linear theory, since as was presented in figure 3.3, for $\alpha \geqslant 1.1$ the laminar flow is linearly stable for every Re. As a consequence there is no change of stability on the laminar flow and hence no bifurcating branch of secondary flows emanates from it. This situation can also be verified in figures 3.9 and 3.10, which will also be commented in §3.4. Likewise, for the same parameters of figures 3.4 and 3.5, figures 3.6 and 3.7 show the speed c at which the observer sees a periodic flow as stationary, according to (3.10). We remark the qualitative difference between those two graphs as a consequence of boundary conditions on pressure or flux.

By simply taking a known travelling wave for some α as initial guess and moving slightly α, we can find periodic solutions for different values of α. These are shown in figure 3.13. In addition in table 3.8 we have computed for several values of α the corresponding minimum value of Re_p and Re_Q for which exists periodic flow. The numerical approximation of the minimum Re follows algorithm (2.44), searching the minimum of $f(\gamma(s)) = \gamma_1 = Re$, as was defined at the beginning of this section. Next, for each α, the minimum Reynolds number $Re_{min}(\alpha)$, is minimized as a function of α by means of an algorithm of minimization without derivatives as

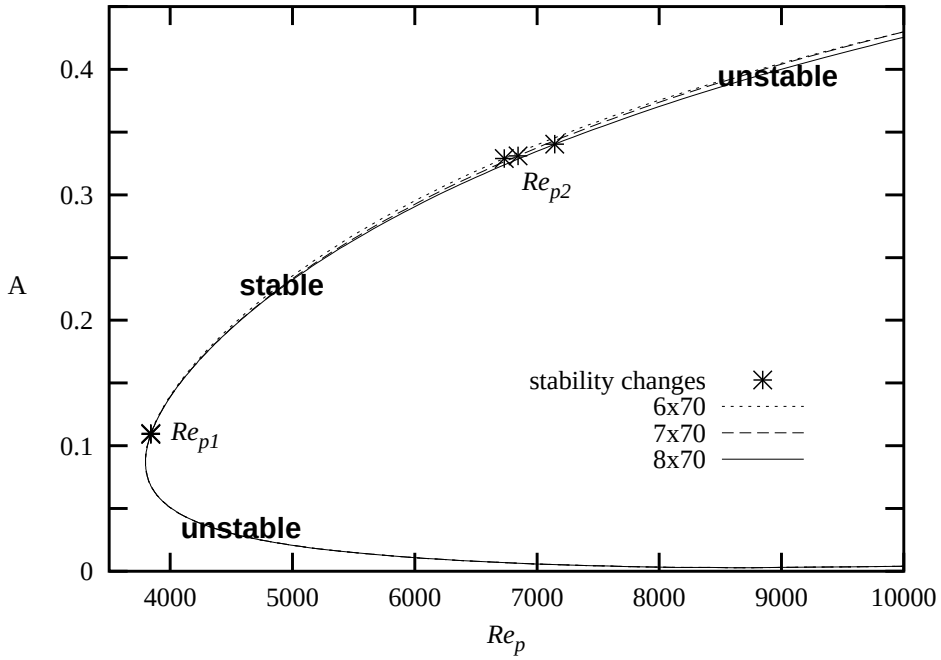

FIGURE 3.4. Bifurcating curve of periodic flows for several discretizations specified as $N \times M$, $\alpha = 1.1$, and based on Re_p. On each curve there are two '*' corresponding to Hopf bifurcations. They divide the different regions of stability to superharmonic disturbances, which are also labeled in the plot according to its character.

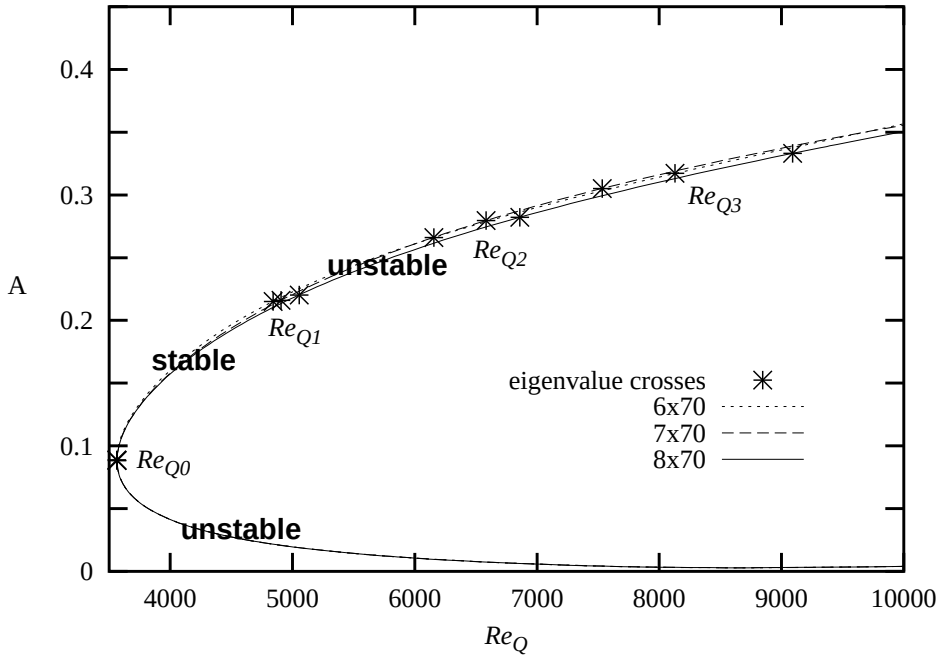

FIGURE 3.5. Analogous of figure 3.4 based on Re_Q. In this case '*' means a real eigenvalue or a pair of complex conjugate eigenvalues which cross the imaginary axis. For each spatial discretization three Hopf bifurcations are presented on the upper branch, in addition to the change of stability at the minimum Re_Q. From the first Hopf bifurcation on the upper branch the secondary flows are unstable.

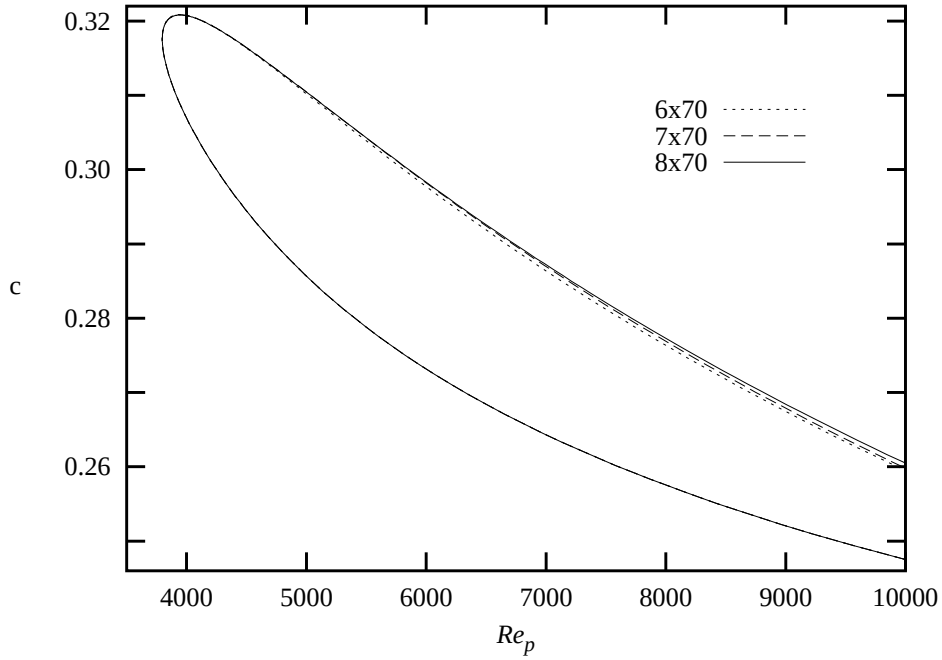

FIGURE 3.6. Speed of the observer for parameters and periodic solutions as in figure 3.4. Upper and lower branch corresponds to the respective branch of amplitudes.

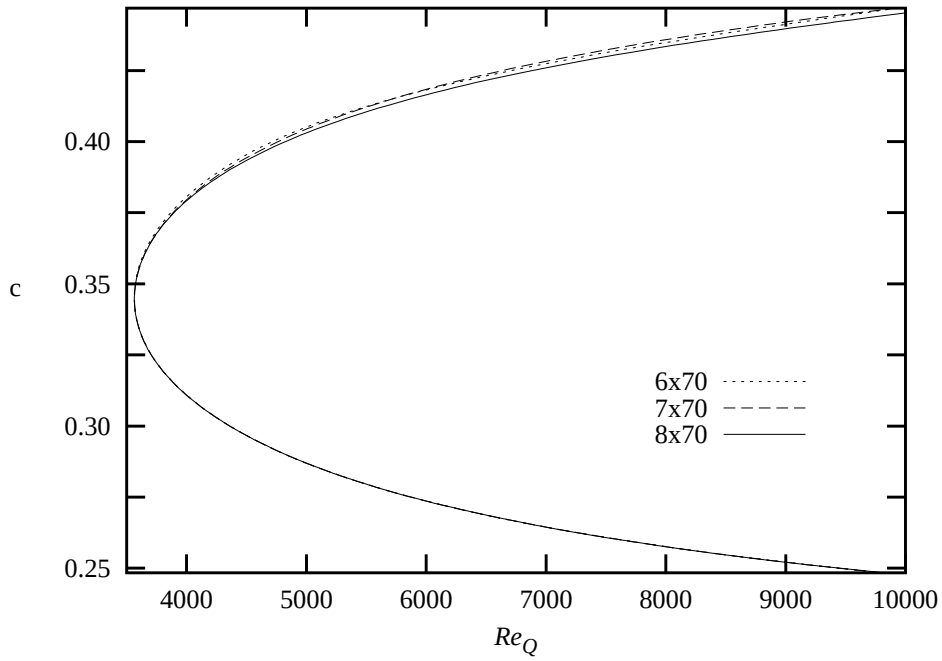

FIGURE 3.7. Analogous of figure 3.6 based on Re_Q. Unlike the case of Re_p, the upper branch increases with Re_Q.

described in §2.9. In this way we obtain the minimum Re_p and Re_Q for which there exists periodic solution. This are marked with '*' in table 3.8. For Re_p, Herbert (1976) obtained the minimum value at $Re_p = 2934.80$ for $\alpha = 1.3231$ and 4×40 as the spectral spatial discretization for the stream function: this discretization is analogous to the one used in the present work. We observe that our results differ from these not more than 0.083%.

α	$\min Re_Q$	α	$\min Re_p$
1.2200	2875.9110	1.2200	3126.9581
1.2500	2767.7741	1.2500	3033.7307
1.3300	2605.2298	1.3206	2933.9739
1.3554	2593.9895	1.3242	2933.7130*
1.3559	2593.9851*	1.3303	2934.4789
1.3560	2593.9853	1.3559	2955.1751
1.3609	2594.4313	1.3609	2962.8150
1.3800	2604.5834	1.3800	3004.3032
1.4300	2703.3500	1.4300	3228.5282

TABLE 3.8. Minimum values of Re_p and Re_Q for which exists periodic flow for some values of α. Calculations made for $N = 4$ and $M = 40$. The minimum Re attained is marked with '*'. Results are in good agreement with those reported by Herbert (1976) for Re_p.

3.4 Stability of periodic solutions

We study the stability of solutions of system (3.12) obtained in § 3.3 by means of continuation methods. With a stable solution it is meant the one for which any small disturbance ultimately decays to zero as the flow evolves in time, whereas if some of those disturbances remain permanently away from zero, it is called unstable. We only consider stability for perturbations of the same wavelength α as the periodic solution being analysed. Solutions of (3.12) can either correspond to stable or unstable time-periodic flows. This aspect is not detected by (3.12).

Obtaining of the analytical Jacobian matrix. To decide whether a T-periodic flow u solution of (3.12) is stable or not we linearize (2.17) around u, as a steady solution for its appropriate $c = L/T$ (see (3.9)), to obtain the eigenvalues of its Jacobian matrix. If all the eigenvalues have negative real parts the periodic flow is stable to disturbances of the same wavenumber α but, if there is an eigenvalue with positive real part the solution is unstable. Let us mention that there is always a zero eigenvalue which corresponds to the lack of uniqueness of the time-periodic flow due to translations, as described in § 3.3.

We now describe some ideas in order to obtain the linear part of system (2.17)

$$\begin{cases} \dot{u}_0 = U_0 \\ \dot{\tilde{u}}_k = (I - P_k T_k)^{-1}(\bar{U}_k - P_k \bar{V}_k), \quad k = 1, \ldots, N, \end{cases}$$

considered as a real system of ODE. The definitions of each term are given in § 2.4. The main difficulties are encountered in derivating the non-linear terms

$$\left[(u-c)\frac{\partial u}{\partial x}+v\frac{\partial u}{\partial y}\right]_p, \qquad \left[(u-c)\frac{\partial v}{\partial x}+v\frac{\partial v}{\partial y}\right]_p,$$

for $p=0,\ldots,N$. Following notation of § 2.4 we put $U=(u_0,\bar{u}_1,\ldots,\bar{u}_N)$ and then the term $f(U)=[(u-c)\partial u/\partial x]_{pm}$ for $p=0,\ldots,N$, $m=1,\ldots,M-1$, can be expressed as $f(U)=(f_2\circ f_1)(U)$, for

$$\begin{aligned}
f_1(U) &= (u_{0m}, u^r_{1m}, u^i_{1m}, \ldots, u^r_{Nm}, u^i_{Nm},\\
&\qquad 0\alpha u_{0m}, -1\alpha u^i_{1m}, 1\alpha u^r_{1m}, \ldots, -N\alpha u^i_{Nm}, N\alpha u^r_{Nm})\\
f_2(u_{0m}, u^r_{1m}, u^i_{1m}, \ldots, u^r_{Nm}, u^i_{Nm}, v_{0m}, v^r_{1m}, v^i_{1m}, \ldots, v^r_{Nm}, v^i_{Nm}) &= \sum_{k=p-N}^{N} u_{km}v_{p-k,m}\\
&= \sum_{k=0}^{N-p} u^*_{km}v_{p+k,m} + \sum_{k=1}^{p} u_{km}v_{p-k,m} + \sum_{k=p+1}^{N} u_{km}v^*_{p-k,m},
\end{aligned}$$

where the superindex r and i stands for real and imaginary parts respectively, '*' denotes complex conjugate and we have supposed u and v to be real functions. The last term in the expression of f_2 is defined only for $p<N$. According to § 2.4, $\bar{v}_k=T_k\bar{u}_k$ for $k=1,\ldots,N$. Combining this fact with the partial derivatives of f_1 and f_2 we can obtain the gradient of f. Even though it is a tedious procedure, there is no significant differences in derivating the remaining non-linear terms.

Numerical results. In the bifurcating diagram of periodic flows in figures 3.4 and 3.5 appear several Hopf bifurcations marked with '*', as well as the stability regions which those bifurcations give rise to. Analogous bifurcations are presented in figure 3.13 for Re_p and several values of α.

Now let us discuss the bifurcation diagram shown in figure 3.13 for $\alpha=1.02056$. For the case of the laminar flow, we obtain the classical results of Orszag (1971) about the critical Reynolds being at $Re_{cr}=5772.22$, where the transition from stable to unstable laminar flow takes place, and what was formerly presented in figure 3.3. On the one hand, the bifurcation curve of periodic flows reaches the laminar solution at the above mentioned Re_{cr} and in addition, the laminar solution is checked to be stable when $Re_p<Re_{cr}$ and unstable if $Re_p>Re_{cr}$. At this point the laminar flow has a Hopf bifurcation, that gives rise to a unstable family of periodic orbits. This family continues backwards (with respect to the Reynolds number) until $Re_p\approx 4660$, when a turning point is reached. Before arriving at this turning point (see figure 3.14), there is a single eigenvalue of the Jacobian matrix on the real positive axis, while the remaining eigenvalues have negative real part. On traversing through the turning point, a real and negative eigenvalue becomes real positive, so the number of unstable eigenvalues is now two. Shortly after that, these two unstable eigenvalues collide and become a conjugate complex pair (still with positive real part), and then they cross the imaginary axis for $Re_p\approx 4700$ producing a new Hopf bifurcation at the point B_1 on figure 3.13. Between $Re_p\approx 4700$ and $Re_p\approx 7400$ (at the point B_2 on figure 3.13), the family of periodic orbits is stable to disturbances of the same wavelength. At $Re_p\approx 7400$, there is another Hopf bifurcation produced by a conjugate pair of eigenvalues crossing the imaginary axis. These bifurcations persist when M, N are increased and no new ones seem to appear in this range.

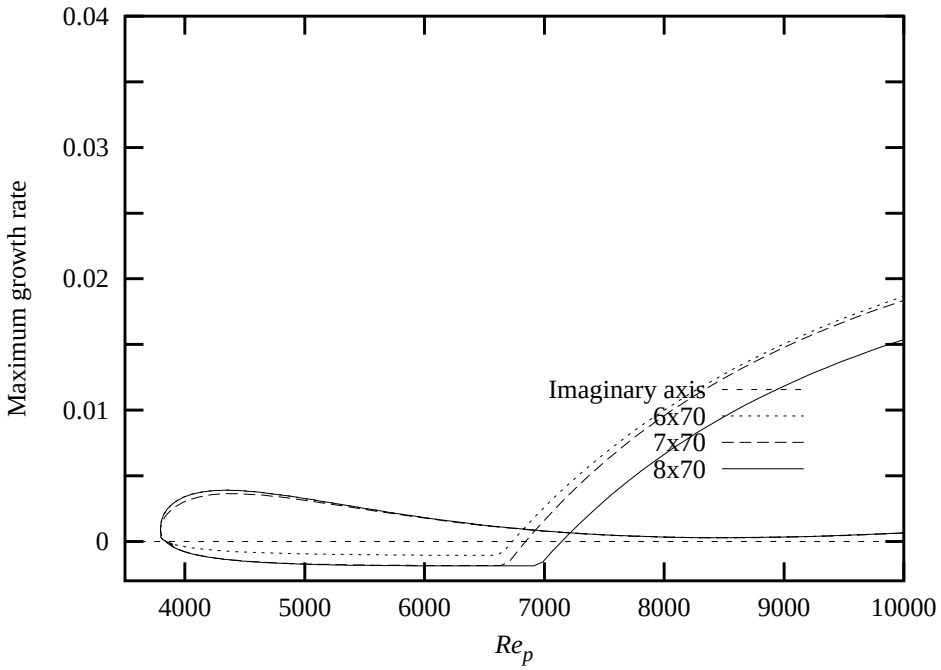

FIGURE 3.9. Real part of the most unstable eigenvalue for periodic flows for $\alpha = 1.1$ and $N \times M$ as specified. The two crossings of each graph with the imaginary axis corresponds to the first two '*' of figure 3.4 and are detailed in table 3.11 as Re_{p1} and Re_{p2}.

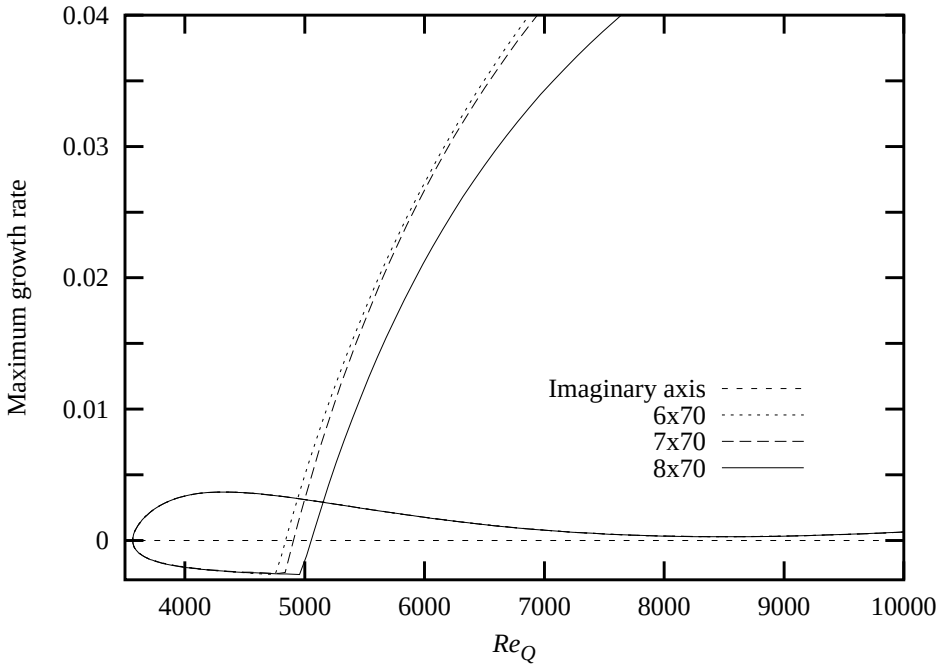

FIGURE 3.10. Analogous of figure 3.9 based on Re_Q. The two crossings of each graph with the imaginary axis corresponds to the first two '*' of figure 3.5 and are specified in table 3.11 as Re_{Q0} and Re_{Q1}.

N	Re_{p1}	c_1	τ_1	Re_{p2}	c_2	τ_2
			Present work for $\alpha = 1.02056$			
4	4701.7	0.29729	9662.43	7450.1	0.28091	17.93
5	4684.6	0.29881	8983.08	6347.5	0.29014	17.39
6	4686.1	0.29868	9080.07	6355.4	0.29013	17.22
7	4684.1	0.29853	9143.27	6643.2	0.28783	17.33
8	4684.1	0.29857	9125.21	6827.8	0.28608	17.49
			Present work for $\alpha = 1.1$			
4	3864.5	0.31927	7427.55	8946.1	0.26985	17.88
5	3841.0	0.32004	7090.00	7670.3	0.28059	16.87
6	3841.4	0.32018	7065.51	6732.7	0.28927	16.59
7	3840.8	0.32010	7100.30	6844.8	0.28863	16.58
8	3840.6	0.32010	7098.79	7145.8	0.28568	16.75
			Soibelman & Meiron (1991) for $\alpha = 1.1$			
2	3630		4742.32	9400		35.50
3	3800		4935.43	9675		17.65
4	3775		4875.63	9592		16.54

TABLE 3.11. Convergence of the two first bifurcating Reynolds numbers for constant pressure and associated parameters c and τ for different α. All of them are given for $M = 70$. The values reported in Soibelman & Meiron (1991) for $M = 70$ are also included.

N	Re_{Q0}	c_0	Re_{Q1}	c_1	τ_1	Re_{Q2}	c_2	τ_2	Re_{Q3}	c_3	τ_3
					Present work for $\alpha = 1.1$						
4	3603.5	0.34248	5812.6	0.41532	11.62	7187.8	0.42910	6.84	7263.9	0.42971	19.38
5	3564.7	0.34467	5296.6	0.40633	11.65	6092.5	0.41686	22.42	6643.0	0.42270	9.81
6	3562.8	0.34506	4840.4	0.40235	11.93	6155.7	0.41979	22.10	8128.2	0.43567	9.80
7	3564.9	0.34475	4905.9	0.40270	11.88	6584.1	0.42448	22.14	7534.2	0.43251	10.06
8	3564.7	0.34474	5054.0	0.40392	11.85	6858.1	0.42477	22.16	9090.6	0.44020	9.94
					Soibelman & Meiron (1991) for $\alpha = 1.1$						
2			5600		20.6	6125		18.6			
3			6250		12.5	7750		20.73			
4			5875		13.4	7500		19.75			

TABLE 3.12. Minimum Reynolds number Re_{Q0} and the first three Hopf bifurcations at Re_{Q1}, Re_{Q2}, Re_{Q3} of periodic flows, together with associated parameters c and τ for $\alpha = 1.1$, $M = 70$ and several N. The values reported in Soibelman & Meiron (1991) for $M = 70$ are also included.

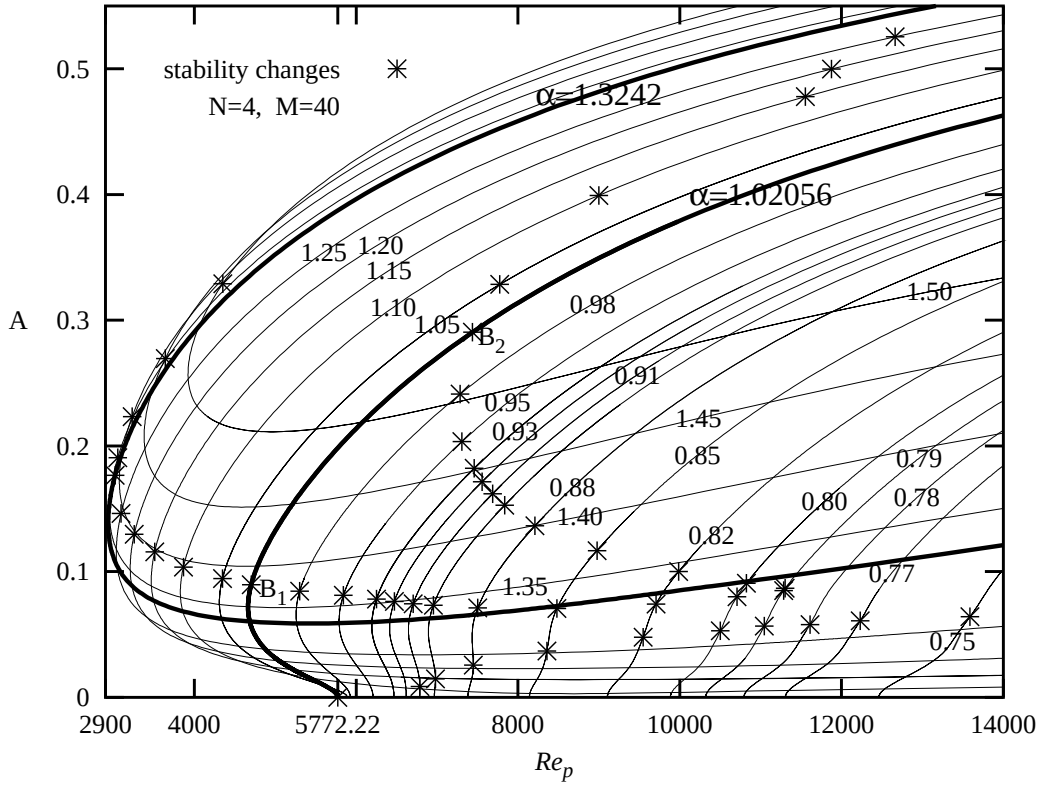

FIGURE 3.13. Bifurcating curves of periodic flows for Re_p and several values of α specified on each curve. The number of discretization points is $N = 4$, $M = 40$. The '*' on each curve represents a Hopf bifurcation. Curves for $\alpha = 1.02056$ and $\alpha = 1.3242$ are traced in bigger dots. For $\alpha = 1.02056$ it is attained the critical Reynolds number at $Re_p = 5772.22$ and for $\alpha = 1.3242$ it is approximately reached a solution at a minimum $Re_p = 2934$.

The case of constant flux is qualitatively different. For Re_Q the bifurcating diagram of periodic solutions has a turning point at a minimum value of Re_Q, which we designate as Re_{Q0}. The lower branch of periodic solutions is unstable with only one unstable real eigenvalue and the upper initially stable, being also real the most unstable eigenvalue. On traversing the bifurcating curve towards the upper branch (see figure 3.5), this real positive eigenvalue that becomes negative at the turning point. The upper branch is kept stable until a subsequent Hopf bifurcation appears at certain value Re_{Q1}. Further on Re_Q we have obtained two more Hopf bifurcations at points called Re_{Q2} and Re_{Q3}. Unlike the case of constant pressure, if we keep increasing Re_Q the situation becomes more complicated as new Hopf bifurcations appear. For $N = 8$ and $Re_Q \approx 10000$ we have detected a total of 5 Hopf bifurcations. In spite of the lack of convergence in the number and location of the bifurcations, a qualitatively similar behaviour has been observed for all the spatial discretizations considered up to $N = 8$.

The maximum growth rate (the real part of the most unstable eigenvalue) for each periodic flow is presented in figures 3.9 and 3.10 for the same parameters as figures 3.4 and 3.5. This diagram represents the degree of instability of each flow. For Re_Q and λ the most unstable eigenvalue, $\mathrm{Re}(\lambda)$ crosses the imaginary axis twice, on the values Re_{Q0} and Re_{Q1}.

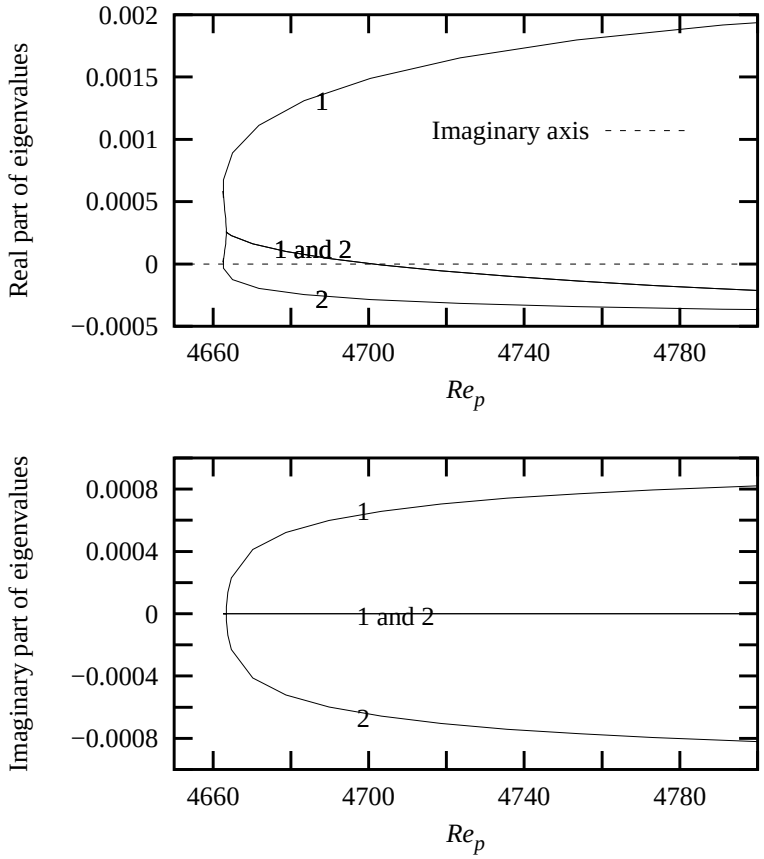

FIGURE 3.14. Real and imaginary part of the two most unstable eigenvalues (labeled 1 and 2) of periodic flows for $N = 4$, $M = 40$, $\alpha = 1.02056$ and Re_p. At the minimum Re_p of the curve two unstable real eigenvalues give rise to a pair of complex conjugate eigenvalues. The first crossing of the real part through the imaginary axis corresponds to a real eigenvalue, meanwhile the second one corresponds to a Hopf bifurcation.

Pugh & Saffman (1988) pointed out that the null eigenvalue at Re_{Q0} has algebraic multiplicity 2 and geometric multiplicity 1. We can consider that eigenvalue simple (with algebraic and geometric multiplicity 1) if we ignore the constant zero eigenvalue due to a trivial phase shift of the flow in the stream direction (see beginning of §3.3). The suppression of this trivial null eigenvalue can be made by restricting equations (2.17) to the closed linear manifold Σ_1 defined as a Poincaré section in §2.7. According to bifurcation theory (see Perko 1998, p. 334) at a simple eigenvalue, we have no equilibrium point for $Re_Q < Re_{Q0}$ and two equilibrium points for $Re_Q > Re_{Q0}$: this is then a saddle-node bifurcation and no new branches of solutions come out from Re_{Q0}.

Formulas (1.10) or (1.11), together with (1.12) provide the correspondence between bifurcation points at Re_Q and Re_p. For instance the periodic solution at Re_{Q0} for $N = 8$, $M = 70$ and $\alpha = 1.1$, transformed by these formulas furnish a periodic solution at $Re_p = 3839.4$ and $c = 0.32008$, values which are in good agreement with Re_{p1} as reported in table 3.11. Likewise, the transformed periodic solution at Re_{Q1} gives rise to $Re_p = 7145.91$ and $c = 0.28568$, again with good precision with respect to table 3.11.

Previously, Soibelman & Meiron (1991) found analogous bifurcations of travelling waves for

$\alpha = 1.1$, and the critical Reynolds number for which there are time-periodic solutions: $Re_p \approx 2900$ for $\alpha \approx 1.3$, and $Re_Q \approx 2600$ (they do not report α for Re_Q). We remark that in figure 3.13 there exists an attracting periodic solution for $Re_p \approx 3000$ and $Re_Q \approx 2600$. For $\alpha \gtrsim 1.1$ the curve of periodic solutions does not reach the laminar flow. This is in agreement with the situation in figure 3.3, since for $\alpha \gtrsim 1.1$ the laminar flow is linearly stable for every Re. In figure 3.13 we also observe that for $\alpha \gtrsim 0.91$ the curve of periodic flows bifurcates subcritically from the laminar flow, but for $\alpha \lesssim 0.91$ the Hopf bifurcation is changed into supercritical and at that point it is born a new Hopf bifurcation on the curve of travelling waves.

In tables 3.11 and 3.12 are shown Re_p, Re_Q, the speed of the observer c and the period τ of the bifurcated solution corresponding to the first Hopf bifurcations for several values of N and $M = 70$. Taking $M = 70$ Chebyshev modes seem to be enough to attain convergence in the results. The values obtained by Soibelman & Meiron (1991) are also presented for comparison. For $\alpha = 1.1$ we observe convergence of our results on Re_{p1} and Re_{Q0} as N is increased. Instead, for $N = 8$ we have not yet achieved convergence on the remaining bifurcations. In all cases there are substantial differences with Soibelman & Meiron's (1991) results, being in more agreement for the lowest Re. We remark the slow convergence on the Fourier series as N is increased.

3.5 Unstable invariant manifolds

In our study of the dynamics of plane Poiseuille flow, we are going to analyse the connection between different configurations of the flow. We want to know how the fluid evolves and to which kind of solution it is conducted when it starts on an unstable periodic solution, as the ones found in § 3.3. We have selected several flows for $\alpha = 1.02056$ and $\alpha = 1.1$, taking for the spatial discretization $N = 8$ and $M = 70$ and for the temporal one $\Delta t = 0.02$. Those flows have one real unstable eigenvalue or a couple of complex conjugate unstable eigenvalues. All the solutions on the lower branch of figures 3.4 and 3.5 belong to the first group. In the case of constant pressure, the arc of the upper branch before Re_{p1} and after Re_{p2} for $Re_p < 14000$, correspond to the second group. On the other hand, for Re_Q, only the arc between Re_{Q1} and Re_{Q2} belongs to the second group. For each of these periodic flows $u^p(x, y, t)$, we have studied its unstable manifold and which new state of the fluid they are connected to. By means of the Jacobian matrix computed in §3.4 we can obtain the eigenvector $w \in \mathbb{C}^K$ (K as defined in §3.3) associated with the unstable eigenvalue. The perturbed flow $u^p + rw$ for $|r| \ll 1$ is thus a first order approximation of the unstable manifold of u^p, which in turn is an attracting manifold. We have followed the temporal evolution of $u^p + rw$ until an attracting state is reached. In the case that u^p has only one real unstable eigenvalue, we have considered two ways of escaping from u^p for $r > 0$ or $r < 0$. When there is a couple of complex conjugate eigenvalues, we have chosen an arbitrary direction in the plane generated by the real and imaginary parts of w.

In figures 3.17–3.34 each point corresponds to two selected coordinates (956 and 210 to be precise) of the solution vector $(u_0, \bar{u}_1, \ldots, \bar{u}_N)$ (defined in §2.4) when the flow crosses Σ_1 (defined in § 2.7). For instance, on Σ_1 the evolution of a stable periodic flow is represented by a constant point on those figures and the laminar flow by coordinates $(0, 0)$. In figures 3.17–3.20 and 3.22 we present different situations where the unstable manifold of the periodic solution is connected either with the laminar solution or with a periodic one. In figure 3.21 the unstable periodic flow for $Re_p = 9921$, on the uppper branch of the amplitude diagram, is directed to an attracting quasi-periodic flow with 2 frequencies (the subject of chapter 4), which is observed in this figure

$\alpha = 1.02056$		$\alpha = 1.10$		$\alpha = 1.10$	
Re_p	attractor	Re_p	attractor	Re_Q	attractor
4638	laminar	3803	laminar	5264	2-torus
4654*	laminar	3816	laminar	5402*	2-torus
4680	laminar	3835*	laminar	5601*	2-torus
6952	2-torus	7268	2-torus	5801*	2-torus
7184	2-torus	7615	2-torus	6069	2-torus
7438	2-torus	7991	2-torus	6321	2-torus
7713	2-torus	8398	2-torus	6589	2-torus
8012	2-torus	8839	2-torus	6682	2-torus
8336	2-torus	9316	2-torus	6776*	2-torus
8688	2-torus	9832	2-torus		
9067	2-torus	10388	2-torus		
9478	2-torus	10990	2-torus		
9921*	2-torus	11638	2-torus		
10398	2-torus				
10912	2-torus				

TABLE 3.15. Attractors of the flow to which is connected the unstable manifold of periodic solutions on the upper branch of the amplitude curve. In all cases $N = 8$ and $M = 70$.

as an almost closed curve (see the caption of the figure for an explanation). A similar situation is presented in figure 3.23 for a periodic flow on the lower branch for $Re_p = 9094$, very close to the laminar solution, which is again attracted by a quasi-periodic flow enlarged in figure 3.24. Analogously in figures 3.25–3.28 the unstable perturbed periodic flow on the upper branch is attracted by a quasi-periodic solution. On the other hand, in figure 3.29, u^p corresponds to a periodic flow for $Re_Q = 5822$ on the lower branch. The unstable manifold of this solution is connected first with the periodic flow on the upper branch. Since this flow is unstable, the fluid is driven to another attracting flow which, in this case, turns out to be a quasi-periodic flow with 2 frequencies, belonging to the family considered in chapter 4. Similarly, figure 3.30 starts with u^p on the upper branch for $Re_Q = 6776$ and the flow is again attracted by a quasi-periodic flow with 2 frequencies. However u^p on the lower branch, for $Re_Q = 8389$ in figure 3.31, is attracted by a 3-torus. We verify this by plotting the same two selected coordinates of $(u_0, \bar{u}_1, \ldots, \bar{u}_N)$ when the flow crosses Σ_1 if, in addition, it is approximately on Σ_2, which is another Poincaré section (see (4.4)), defined in an analogous way to Σ_1 for another appropriate coordinate of the solution vector. We observe in figure 3.32 several closed curves which seem to indicate that the new attracting flow lives in a 3-torus. In figure 3.33 for $Re_Q = 8682$, the perturbed unstable periodic flow is first driven to a unstable strange set and finally to another strange set. In the case represented in figure 3.34 for $Re_Q = 9363$, u^p on the lower branch is attracted by an apparently more complex set with larger amplitude. The different configurations obtained for several values of Re_p, Re_Q and α are summarized in tables 3.15 and 3.16. The attractors presented in table 3.16 are obtained in one direction of the unstable manifold. On the other direction the attractor is the laminar solution, except for a few cases. For $Re_Q = 5822$, $\alpha = 1.1$, both directions of the unstable manifold are connected with a 2-torus. For $Re_p = 5772$, $\alpha = 1.02056$, both directions of the unstable manifold

$\alpha = 1.02056$		$\alpha = 1.10$		$\alpha = 1.10$	
Re_p	attractor	Re_p	attractor	Re_Q	attractor
4636	laminar	3802	laminar	3658	periodic
4649*	laminar	3885	periodic	3694	periodic
4689	laminar	3969	periodic	3816	periodic
4722	laminar	4172	periodic	4020	periodic
4766*	periodic	4570	periodic	4559	periodic
4821	periodic	4872	periodic	4611	periodic
4890	periodic	5272	periodic	4814	periodic
4975	periodic	5789	periodic	5101*	2-torus
5079	periodic	6397	periodic	5500	2-torus
5205	periodic	6917	periodic	5822*	2-torus
5361	periodic	7813	2-torus	6049	2-torus
5554	periodic	8192	2-torus	6499	2-torus
5772*	periodic	8642	2-torus	6791	2-torus
		9094*	2-torus	7097	2-torus
		9489	2-torus	7359	2-torus
		9589	unknown	7639	2-torus
		10513	2-torus	7995	3-torus
		11078	laminar	8389*	3-torus
		11375	2-torus	8682*	unknown
				9045	unknown
				9363*	unknown
				9589	unknown
				9848	unknown
				10139	unknown
				10390	unknown
				10746	unknown
				11096	unknown
				11395	unknown

TABLE 3.16. Attractors of the flow to which is connected the unstable manifold of periodic solutions on the lower branch of the amplitude curve. In all cases $N = 8$, $M = 70$ and $\Delta t = 0.02$. The attractors on the table corresponds to one direction of the unstable manifold. On the opposite direction the attractor is the laminar solution, except for a few cases. See the text for details. The temporal evolution is presented in figures 3.17–3.34 for Re marked with '*' in the table.

are connected with the periodic flow on the upper branch as is shown in figures 3.20 for one of them.

For the case of Re_p, $\alpha = 1.02056$, the lower branch is connected with the laminar flow for $Re_p \lesssim 4722$, and with a periodic solution for $4766 \lesssim Re_p \lesssim 5772$. For the case of Re_p, $\alpha = 1.1$, the connection of the lower branch is with the laminar flow for $Re_p \lesssim 3802$, with a periodic flow for $3885 \lesssim Re_p \lesssim Re_{p2}$, with a 2-torus for $Re_{p2} \lesssim Re_p \lesssim 9500$, and with different configurations for $Re_p \gtrsim 9500$. For Re_Q, $\alpha = 1.1$, the lower branch is connected with

a periodic solution for $Re_Q \leqslant Re_{Q1}$, with a 2-torus for $Re_{Q1} \leqslant Re_Q \lesssim 7950$, with a 3-torus for $7950 \lesssim Re_Q \lesssim 8500$, and with unknown sets for $Re_Q \gtrsim 8500$. In this case, for $Re_Q \geqslant Re_{Q1}$ the perturbed unstable periodic flow is first connected with the periodic solution on the upper branch and then is directed to the final attractor. The upper branch is connected with the laminar flow for $Re_p \leqslant Re_{p1}$, and with a 2-torus for $Re_{p2} \leqslant Re_p \leqslant Re_{p3}$, for $\alpha = 1.02056$ and, $\alpha = 1.1$, being Re_{p3} the next Hopf bifurcation after Re_{p2}. For the case of Re_Q, $\alpha = 1.1$, the upper branch is also connected with a 2-torus for $Re_{Q1} \leqslant Re_Q \leqslant Re_{Q2}$.

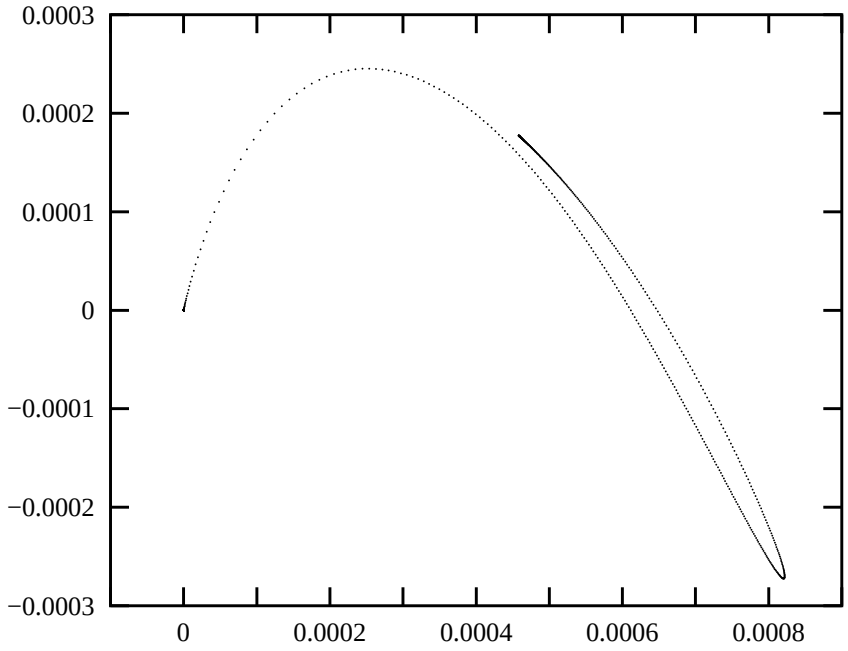

FIGURE 3.17. Two selected coordinates of the solution vector when the flow crosses Σ_1. The perturbed unstable periodic flow on the lower branch for $Re_p = 4649$, $\alpha = 1.02056$ initially increases amplitude and finally falls to laminar. The integration time on the graph is around $32{,}000$ time units.

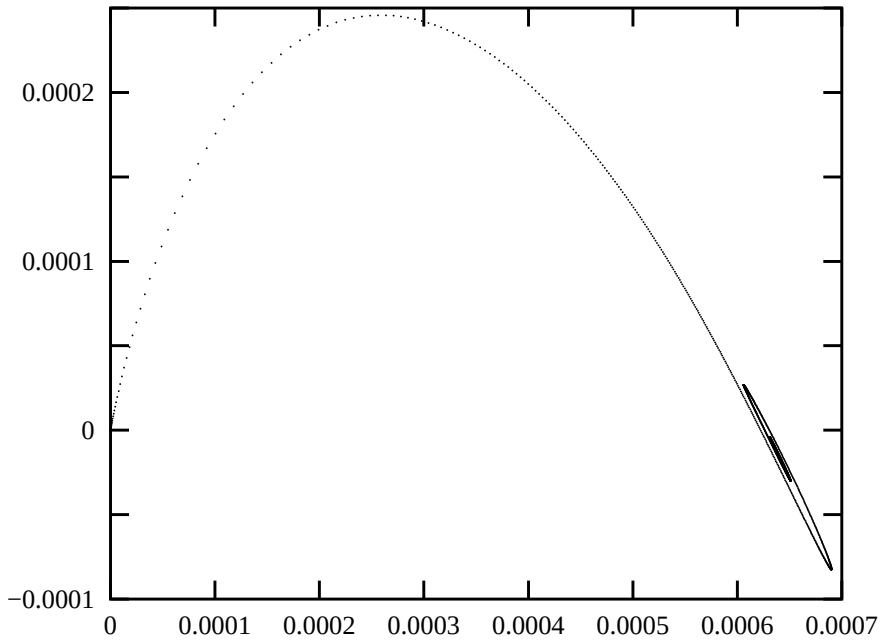

FIGURE 3.18. The perturbed unstable periodic flow on the upper branch for $Re_p = 4654$, $\alpha = 1.02056$, influenced by the near Hopf bifurcaction, initially spirals and finally falls to laminar. In the graph there are plotted around $63{,}000$ time units.

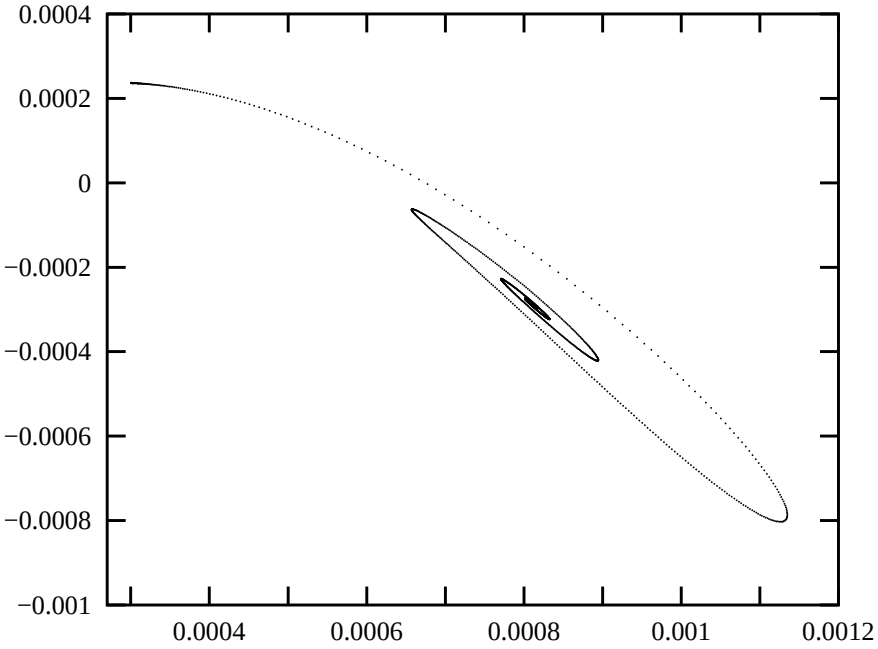

FIGURE 3.19. The solution escapes quickly from the perturbed unstable periodic flow on the lower branch for $Re_p = 4766$, $\alpha = 1.02056$ and, influenced by the near Hopf bifurcaction, spirals, increases amplitude and finally falls to the periodic solution on the upper branch. The integration time plotted is around $53{,}000$ time units.

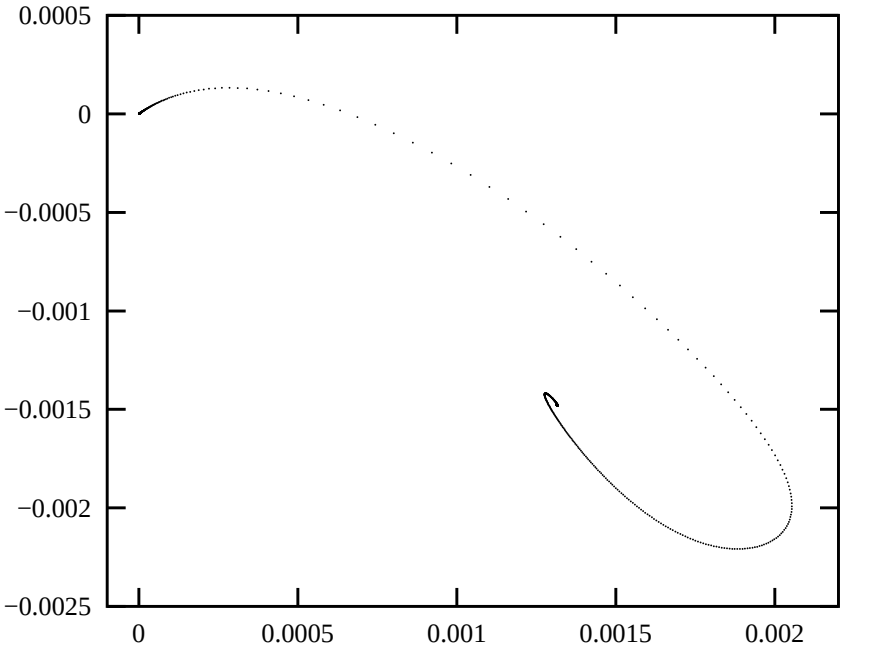

FIGURE 3.20. For $Re_p = 5772$, $\alpha = 1.02056$ the perturbed unstable periodic flow on the lower branch initially departs very close to laminar. At the beginning the amplitude increases very slowly and after the flow escapes far away enough from the initial condition, it is quickly driven to the periodic solution on the upper branch. The integration time on the plot is roughly $242{,}000$ time units.

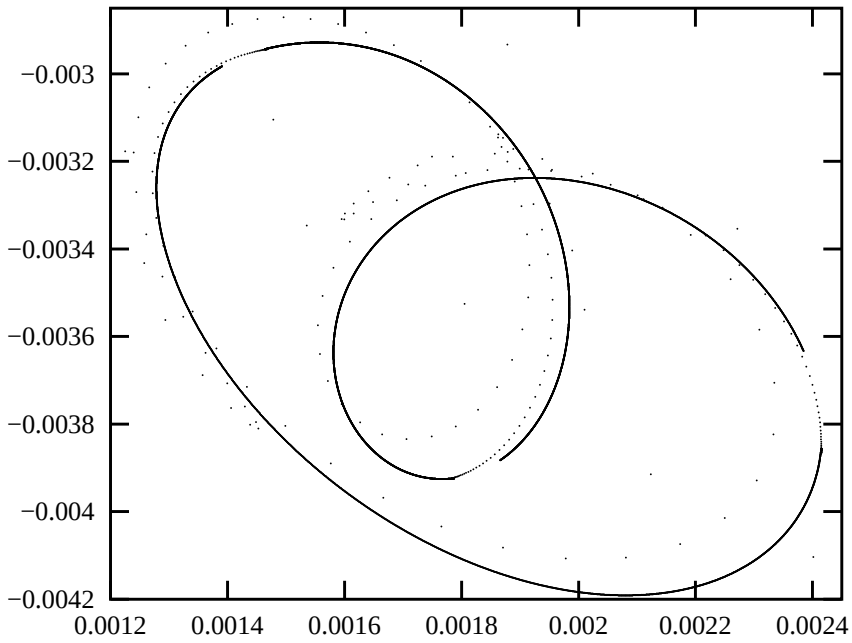

FIGURE 3.21. The perturbed unstable periodic flow on the upper branch for $Re_p = 9921$, $\alpha = 1.02056$, is attracted by a 2-torus, as is shown by the closed curve, which is traced starting from three different points in a continous way: the curve is plotted not closed intentionally to remark this effect. The integration time on the plot is roughly $262{,}000$ time units.

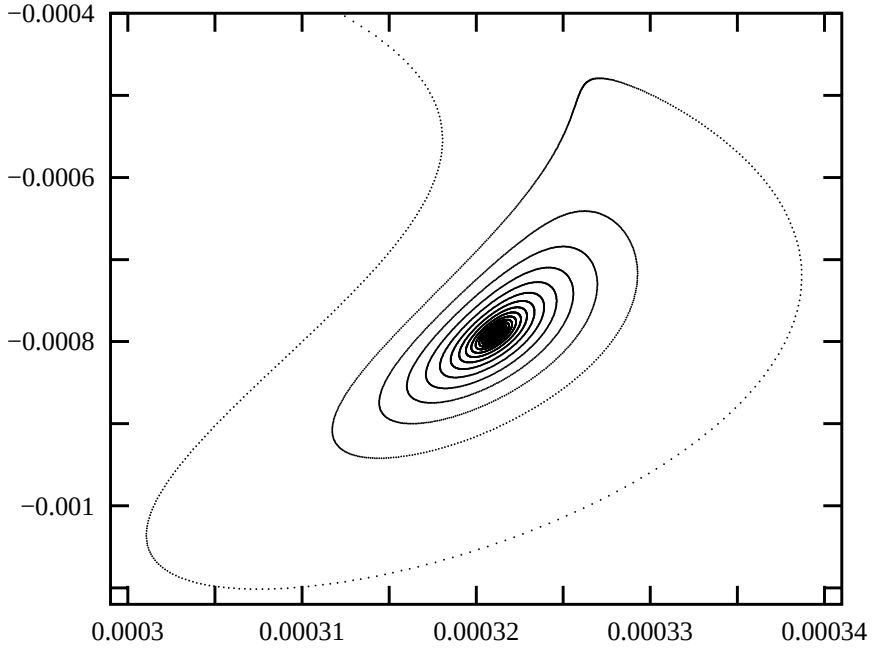

FIGURE 3.22. The flow starts from the perturbed unstable periodic solution on the upper branch for $Re_p = 3835$, $\alpha = 1.10$ and, influenced by the near Hopf bifurcaction, initially spirals while decreases amplitude and finally falls to the laminar solution (this is not shown on the graph). The integration time needed to obain this graph was around $175{,}000$ time units.

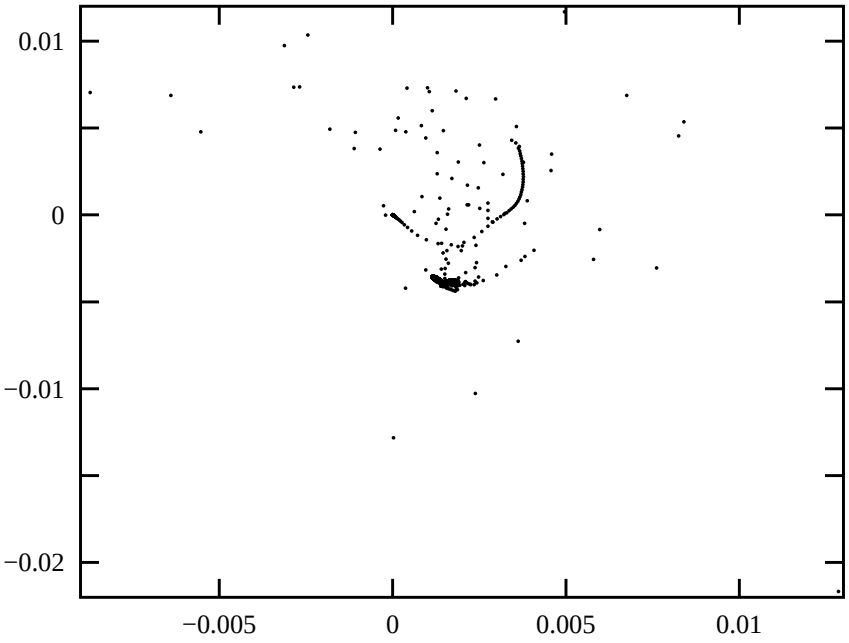

FIGURE 3.23. The perturbed unstable periodic flow on the lower branch for $Re_p = 9094$, $\alpha = 1.10$, departs very close to the laminar flow and is attracted by a 2-torus which is enlarged in figure 3.24. The time represented in the graph is approximately $31{,}000$ time units.

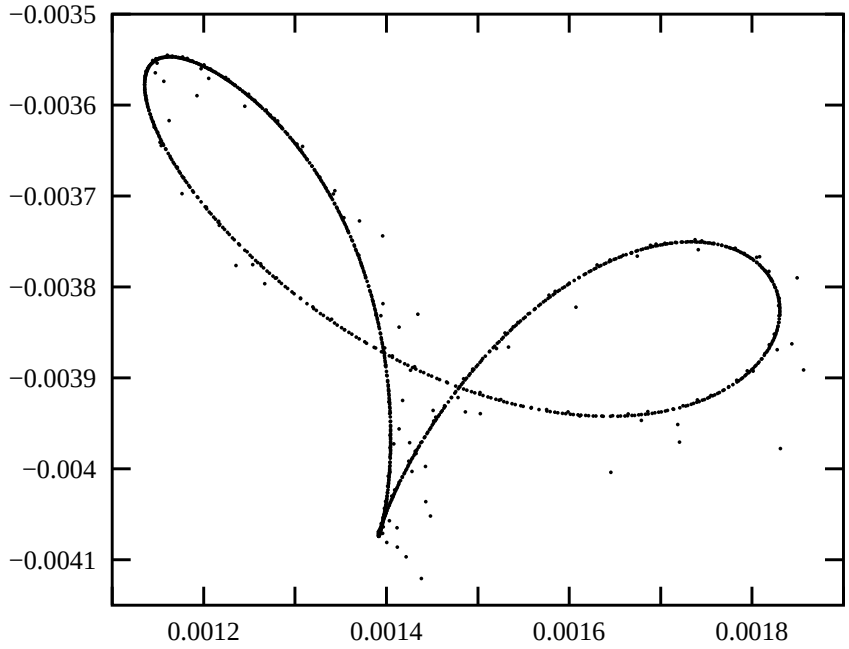

FIGURE 3.24. Enlarging of the attracting 2-torus for $Re_p = 9094$, $\alpha = 1.10$ of figure 3.23.

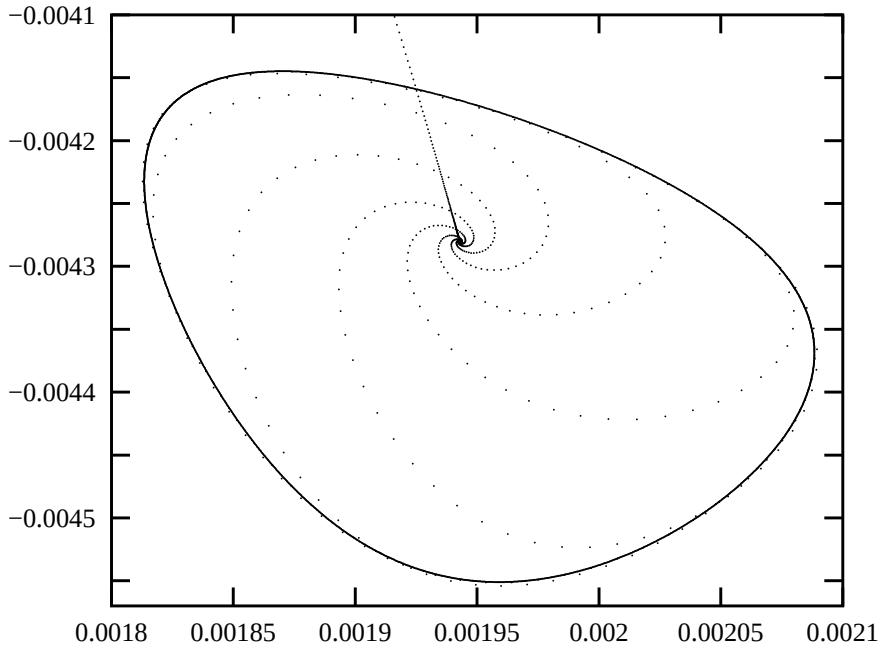

FIGURE 3.25. Final steps of the evolution of the perturbed unstable periodic flow on the lower branch for $Re_Q = 5101$, $\alpha = 1.10$. The fluid is first attracted by the unstable periodic flow on the upper branch, plotted in the centre of the figure. The flow is then driven to a attracting 2-torus. The integration time plotted is around $57{,}000$ time units.

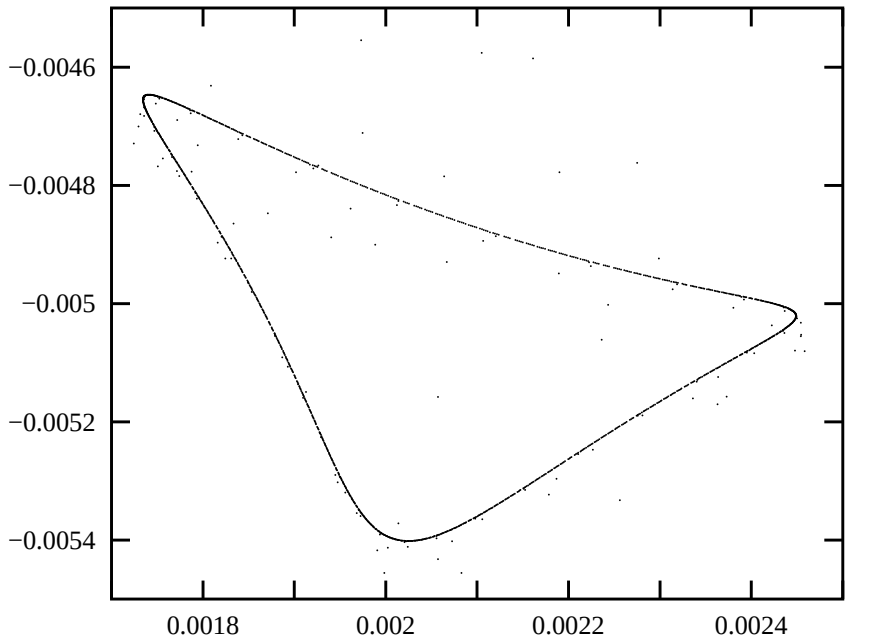

FIGURE 3.26. Flow that starts from the perturbed unstable periodic solution on the upper branch for $Re_Q = 5402$, $\alpha = 1.10$ and is attracted by a 2-torus. The integration time on the figure is about $21{,}000$ time units.

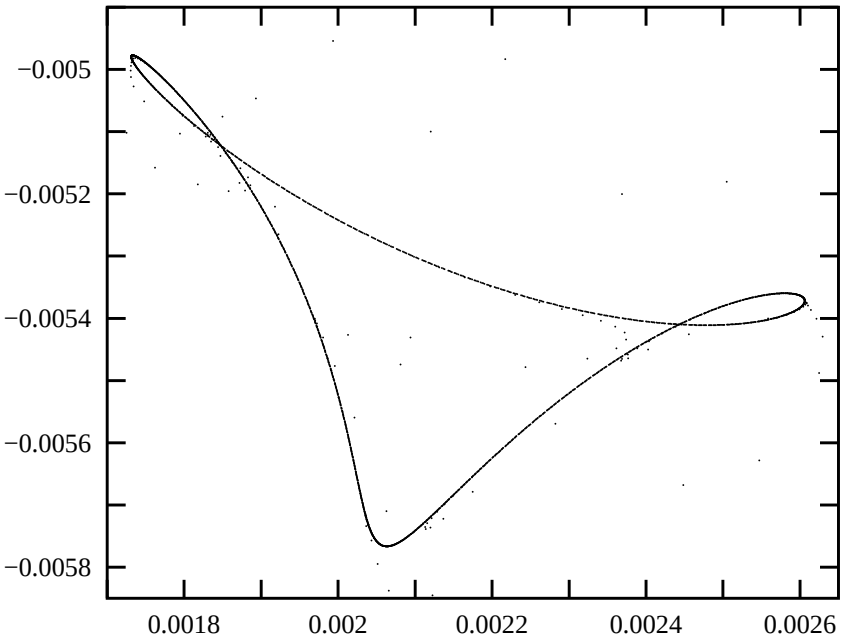

FIGURE 3.27. Flow that starts from the perturbed unstable periodic solution on the upper branch for $Re_Q = 5601$, $\alpha = 1.10$ and is attracted by a 2-torus. The integration time on the figure is about 33,000 time units.

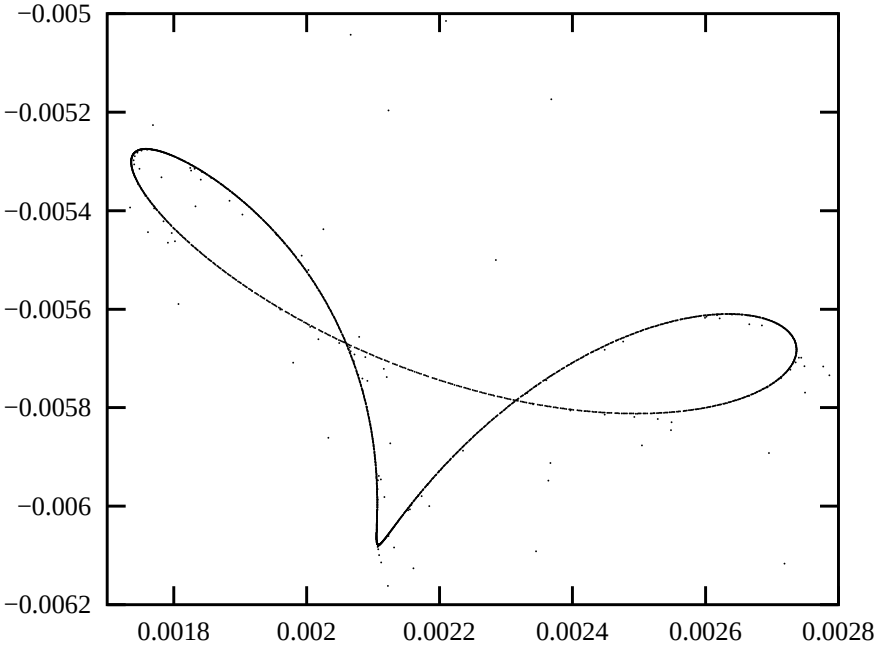

FIGURE 3.28. Flow that starts from the perturbed unstable periodic solution on the upper branch for $Re_Q = 5801$, $\alpha = 1.10$ and is attracted by a 2-torus. The integration time on the figure is about 31,000 time units.

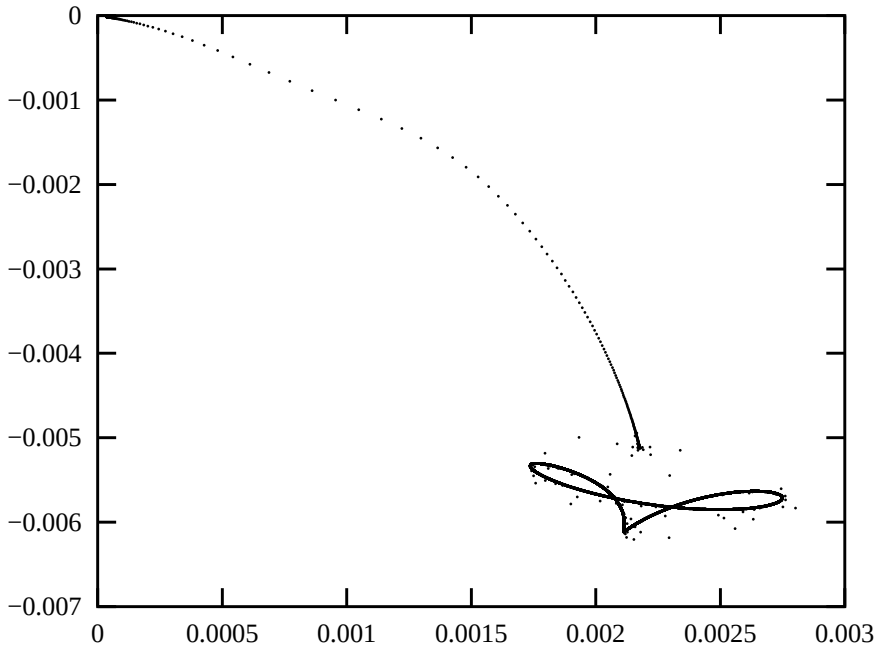

FIGURE 3.29. The initial condition is a disturbance of the unstable periodic flow on the lower branch for $Re_Q = 5822$, $\alpha = 1.10$, which is represented on the figure close to $(0, 0)$. The evolution of the system takes the fluid first to the unstable periodic flow on the upper branch which finally is attracted by a 2-torus with less amplitude. The integration time on the figure is about $195{,}000$ time units.

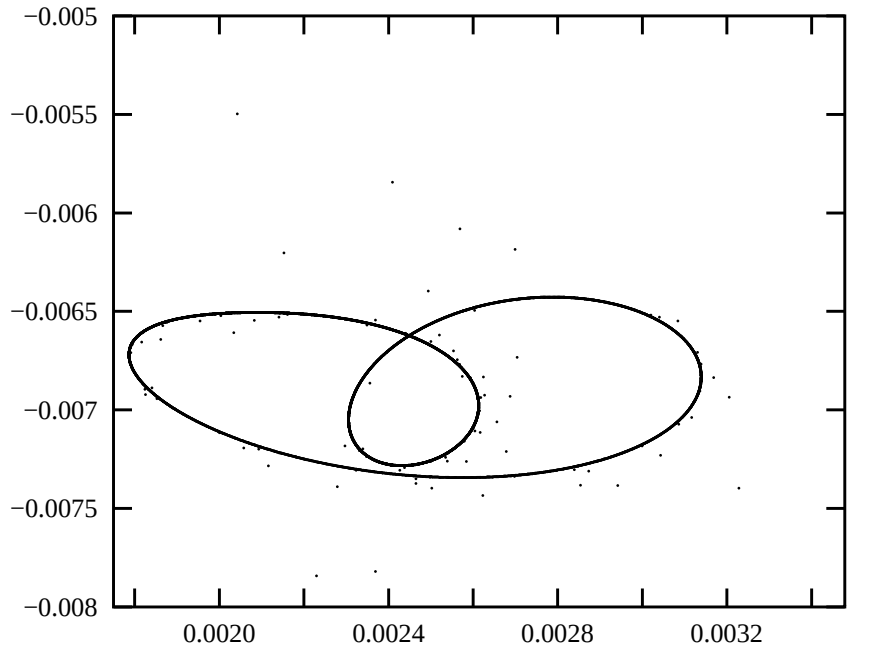

FIGURE 3.30. Flow that starts from the perturbed unstable periodic solution on the upper branch for $Re_Q = 6776$, $\alpha = 1.10$. Its unstable manifold connects this flow with a 2-torus. The integration time on the figure is about $91{,}000$ time units.

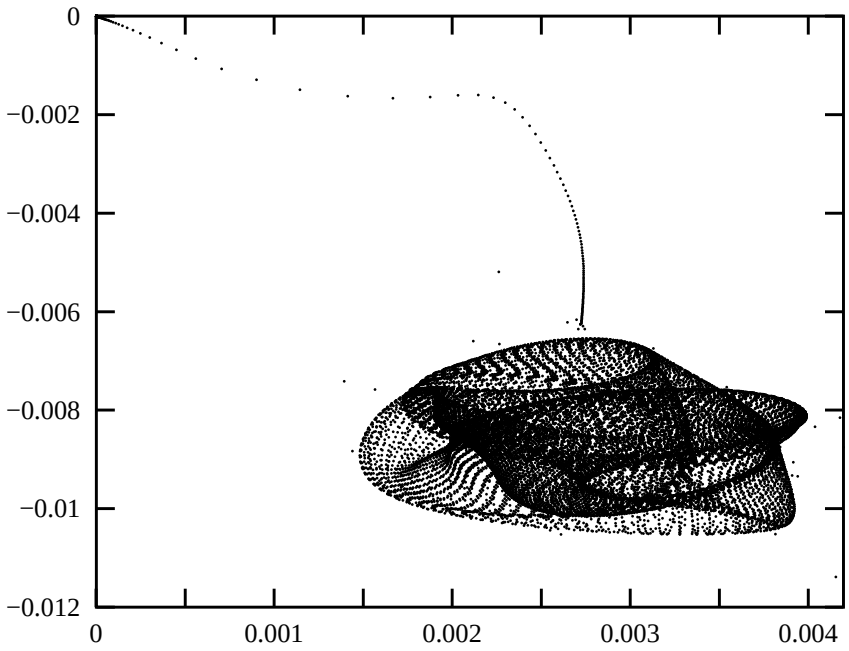

FIGURE 3.31. Flow that starts from the perturbed unstable periodic solution on the lower branch for $Re_Q = 8389$, $\alpha = 1.10$. The flow is first directed to the unstable periodic flow on the upper branch and then attracted by a 3-torus. See also figure 3.32. The integration time on the figure is about $322{,}000$ time units.

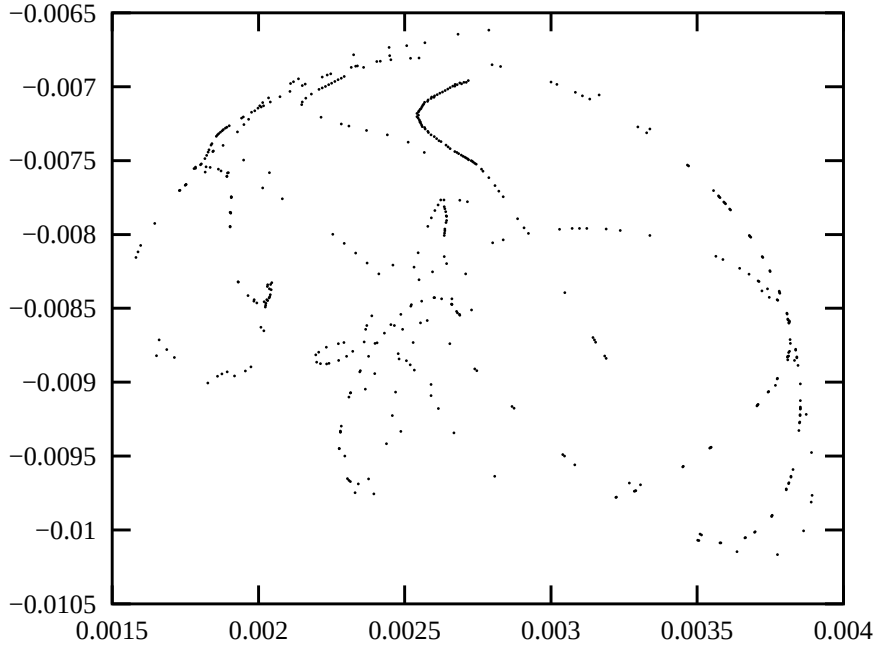

FIGURE 3.32. Attracting flow for $Re_Q = 8389$, $\alpha = 1.10$ of figure 3.31 but the two selected coordinates are only plotted when the solution vector crosses also a second Poincaré section Σ_2. We observe several closed curves, which seem to indicate that the attracting flow is a 3-torus. The integration time on the figure is about $7{,}111{,}000$ time units.

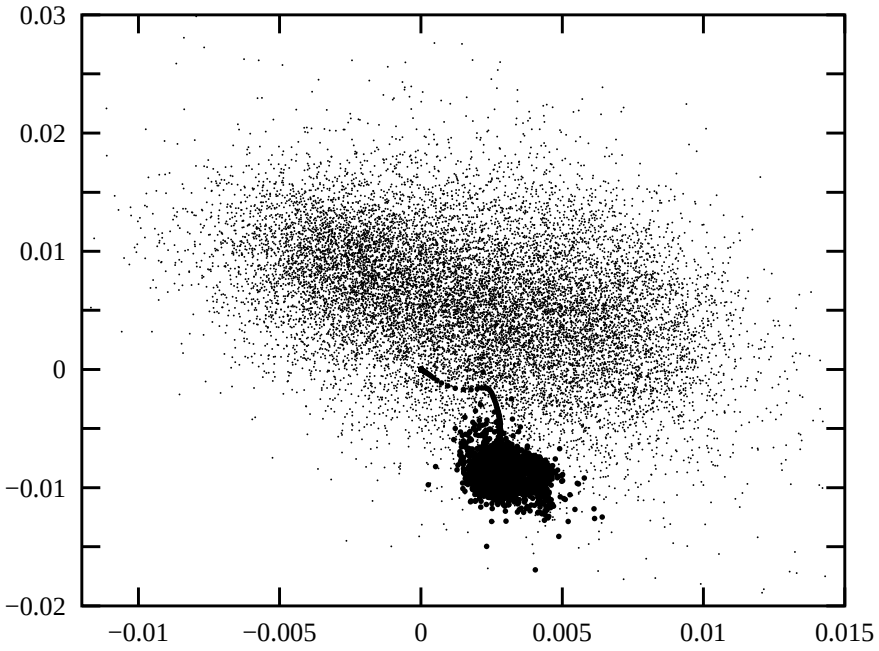

FIGURE 3.33. Flow that starts from the perturbed unstable periodic solution on the lower branch for $Re_Q = 8682$, $\alpha = 1.10$. The flow is attracted by a strange set plotted in bigger dots, which is unstable and finally drives the fluid to another strange set. The integration time on the figure is about $245{,}000$ time units.

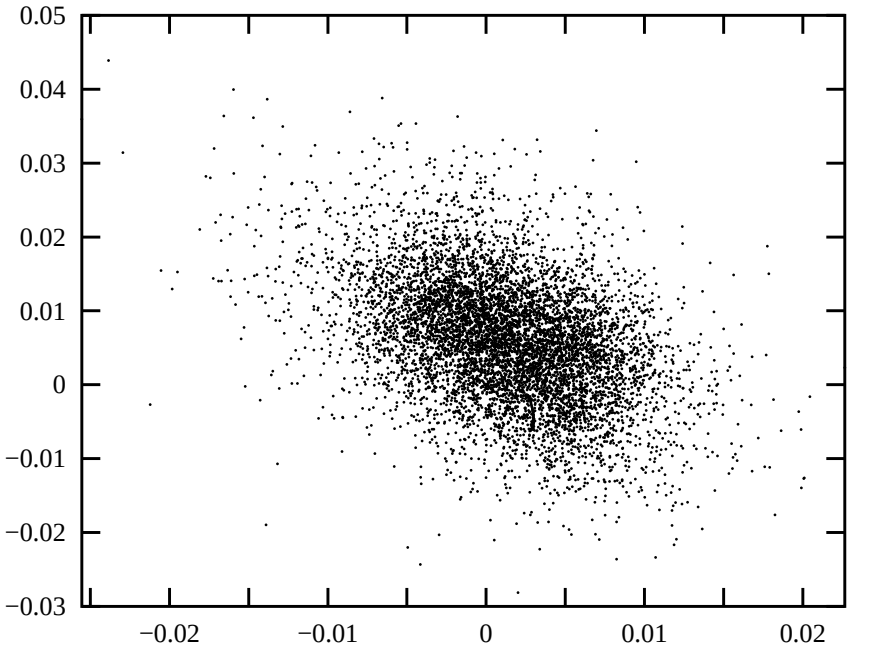

FIGURE 3.34. Flow that starts from the perturbed unstable periodic solution on the lower branch for $Re_Q = 9363$, $\alpha = 1.10$. The flow is attracted by an apparently strange set. The integration time on the figure is about $115{,}000$ time units.